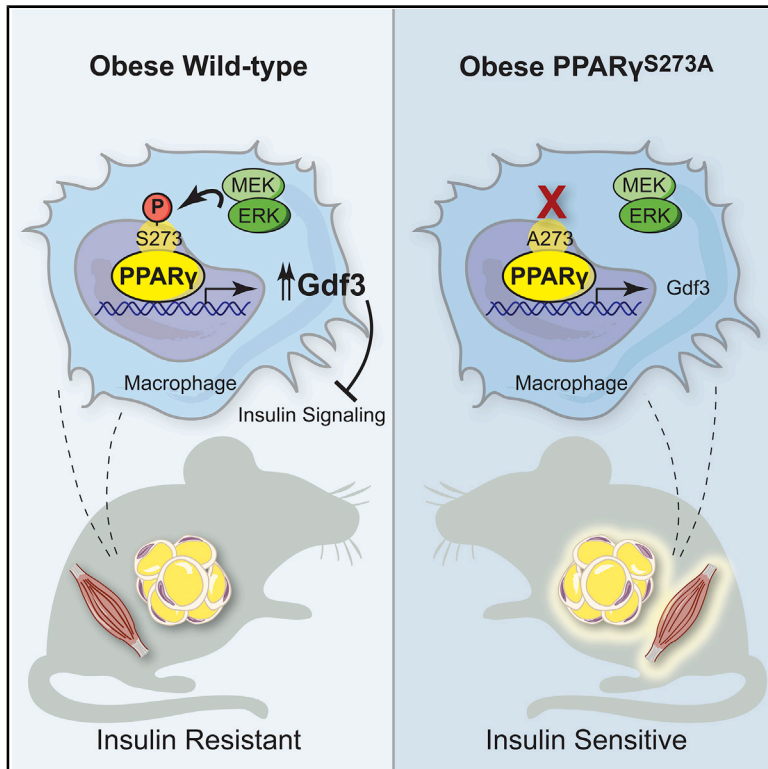


Cell Metabolism

Obesity-Linked PPAR γ S273 Phosphorylation Promotes Insulin Resistance through Growth Differentiation Factor 3

Graphical Abstract



Authors

Jessica A. Hall, Deepti Ramachandran, Hyun C. Roh, ..., Evan D. Rosen, Bruce M. Spiegelman, Alexander S. Banks

Correspondence

asbanks@bidmc.harvard.edu

In Brief

Hall et al. show that mice lacking phosphorylation at serine 273 of PPAR γ are protected from developing insulin resistance in response to high-fat-diet feeding, associated with dramatically reduced levels of Gdf3. Gdf3 in turn is sufficient to cause impaired insulin signaling both *in vitro* and *in vivo*.

Highlights

- Blocking PPAR γ S273 phosphorylation protects mice from insulin resistance in obesity
- These mice do not show the side effects associated with TZD-based PPAR γ agonism
- These mice have reduced expression of Gdf3 mainly in macrophages
- Gdf3 is sufficient to cause impaired glucose homeostasis *in vivo* and *in vitro*



Short Article

Obesity-Linked PPAR γ S273 Phosphorylation Promotes Insulin Resistance through Growth Differentiation Factor 3

Jessica A. Hall,^{1,7} Deepti Ramachandran,^{1,7} Hyun C. Roh,¹ Joanna R. DiSpirito,² Thiago Belchior,¹ Peter-James H. Zushin,¹ Colin Palmer,¹ Shangyu Hong,¹ Amir I. Mina,¹ Bingyang Liu,¹ Zhaoming Deng,¹ Pratik Aryal,¹ Christopher Jacobs,¹ Danielle Tenen,¹ Chester W. Brown,³ Julia F. Charles,⁴ Gerald I. Shulman,⁵ Barbara B. Kahn,¹ Linus T.Y. Tsai,¹ Evan D. Rosen,¹ Bruce M. Spiegelman,⁶ and Alexander S. Banks^{1,8,9,*}

¹Division of Endocrinology, Diabetes and Metabolism, Beth Israel Deaconess Medical Center and Harvard Medical School, Boston, MA 02215, USA

²Department of Immunology, Harvard Medical School, Boston, MA 02115, USA

³Department of Pediatrics, University of Tennessee Health Science Center, Memphis, Memphis, TN 38103, USA

⁴Department of Orthopedics, Brigham and Women's Hospital, Harvard Medical School, Boston, MA 02115, USA

⁵Department of Internal Medicine, Yale University School of Medicine, New Haven, CT 06510, USA

⁶Department of Cancer Biology, Dana-Farber Cancer Institute and Department of Cell Biology, Harvard Medical School, Boston, MA 02215, USA

⁷These authors contributed equally

⁸Twitter: @banksiab

⁹Lead Contact

*Correspondence: asbanks@bidmc.harvard.edu

<https://doi.org/10.1016/j.cmet.2020.08.016>

SUMMARY

The thiazolidinediones (TZDs) are ligands of PPAR γ that improve insulin sensitivity, but their use is limited by significant side effects. Recently, we demonstrated a mechanism wherein TZDs improve insulin sensitivity distinct from receptor agonism and adipogenesis: reversal of obesity-linked phosphorylation of PPAR γ at serine 273. However, the role of this modification hasn't been tested genetically. Here we demonstrate that mice encoding an allele of PPAR γ that cannot be phosphorylated at S273 are protected from insulin resistance, without exhibiting differences in body weight or TZD-associated side effects. Indeed, hyperinsulinemic-euglycemic clamp experiments confirm insulin sensitivity. RNA-seq in these mice reveals reduced expression of Gdf3, a BMP family member. Ectopic expression of Gdf3 is sufficient to induce insulin resistance in lean, healthy mice. We find Gdf3 inhibits BMP signaling and insulin signaling *in vitro*. Together, these results highlight the diabetogenic role of PPAR γ S273 phosphorylation and focus attention on a putative target, Gdf3.

INTRODUCTION

Type 2 diabetes (T2D) is one of obesity's most tightly linked comorbidities, and its prevalence is rising in parallel with the global obesity epidemic (Boden, 1997). T2D results from elevated glycemia consequent to insulin resistance and beta cell failure (Stratton et al., 2000). Although there are several available glucose-lowering agents, few address the underlying pathophysiology of this disease. The thiazolidinediones (TZDs) are a class of insulin-sensitizing anti-diabetic drugs capable of delaying or even preventing the onset of diabetes (DeFronzo et al., 2011). Despite potent insulin sensitization, the clinical use of TZDs has declined due to adverse side effects (Soccio et al., 2014). As ligands for the nuclear receptor peroxisome proliferator-activated receptor- γ (PPAR γ), the therapeutic actions of TZDs have been assumed to result from their classical agonism

toward PPAR γ . This agonism drives adipocyte differentiation and lipogenesis in fat tissues (Lehmann et al., 1995). PPAR γ is most highly expressed in adipose tissue, where it was first characterized as a master regulator of adipocyte differentiation and function (Tontonoz and Spiegelman, 2008). Nonetheless, activation of PPAR γ improves insulin sensitivity owing to its diverse roles in both adipocyte and non-adipocyte cells, including macrophages, T cells, myocytes, and other cell types (Bouhrel et al., 2007; Cipolletta et al., 2012; Hevener et al., 2007; Odegaard et al., 2007). PPAR γ is intimately linked to insulin sensitivity, and genetic variants in the *PPARG* locus associate with diabetes risk (Altshuler et al., 2000; Gouda et al., 2010; Majithia et al., 2014).

We have recently shown that, in addition to PPAR γ agonism, TZDs have a second biochemical role, blocking phosphorylation on PPAR γ at serine 273 (S273) (Choi et al., 2010). Importantly,



phosphorylation of this residue in adipose tissue increases in murine models of obesity, and its reversal correlates with the anti-diabetic effects of TZD administration in obese patients and rodents (Choi et al., 2010; Mayoral et al., 2015). Moreover, synthetic ligands have been generated that prevent PPAR γ S273 phosphorylation in the absence of PPAR γ agonism. These non-agonist PPAR γ ligands exhibit profound glucose-lowering effects with reduced side effects, such as weight gain and fluid retention (Amato et al., 2012; Choi et al., 2011, 2014). Likewise, inhibition of the major protein kinase responsible for PPAR γ S273 phosphorylation, extracellular signal-regulated kinase (ERK), improves insulin sensitivity in obese animals (Banks et al., 2015). Understanding the specific mechanisms linking insulin sensitivity with reversal of obesity-linked PPAR γ S273 phosphorylation is thus attractive as a new therapeutic strategy for T2D, as well as other conditions linked to insulin resistance such as polycystic ovarian syndrome.

Here, we specifically address the contribution of PPAR γ S273 phosphorylation to the development of insulin resistance, using a genetically modified mouse model where PPAR γ cannot be phosphorylated at S273. These data demonstrate that genetic prevention of PPAR γ S273 phosphorylation is an insulin-sensitizing event and is associated with decreased levels of Gdf3 in adipose tissues and skeletal muscle. Gdf3 is therefore a potential biomarker of PPAR γ S273 phosphorylation and insulin resistance. Neutralization of Gdf3 may provide an insulin-sensitizing therapeutic approach.

RESULTS

Improved Insulin Sensitivity in Mice with Non-phosphorylatable PPAR γ S273

Reversal of obesity-linked PPAR γ S273 phosphorylation with small-molecule PPAR γ ligands correlates with anti-diabetic properties in humans and mice. However, it is unknown whether genetic modification of this site will result in chronic improvements in insulin sensitivity. To test this, we have generated a genetic mouse model in which PPAR γ cannot be phosphorylated at S273. Using homologous recombination, a single nucleotide was changed to cause a serine to alanine substitution at codon 273 of PPAR γ (Figures S1A and S1B). Homozygous knockin mice (PPAR $\gamma^{S273A/S273A}$, hereafter referred to as PPAR $\gamma^{A/A}$) were generated using C57BL/6 embryonic stem cells (ESCs) and were born at the expected Mendelian frequencies. Whereas wild-type (WT) mice made obese by exposure to a high-fat diet (HFD) contain PPAR γ that is phosphorylated at S273 in adipose tissue, PPAR γ from PPAR $\gamma^{A/A}$ mice is exclusively unphosphorylated (Figure S1C). PPAR γ S273 phosphorylation increases with progressive obesity (Choi et al., 2010). Consequently, WT mice are predicted to have little PPAR γ phosphorylation in the lean state, rendering them phenotypically identical to lean PPAR $\gamma^{A/A}$ mice. On a standard chow diet, PPAR $\gamma^{A/A}$ mice gain weight similarly, have comparable body compositions, and respond similarly to WT controls in glucose tolerance and insulin tolerance tests (Figures S2A–S2D). Accordingly, in the absence of stimulus to promote PPAR γ phosphorylation, differentiation of primary adipocytes is unchanged between genotypes (Figure S3A). Gene expression of WT and PPAR $\gamma^{A/A}$ primary adipocytes revealed similar mRNA levels of the differentiation markers *Pparg2*,

Fabp4, *Cebpa*, *Lpl*, and *Cd36* (Figure S3B). These data confirm earlier work that modulation of PPAR γ S273 phosphorylation is neither necessary nor sufficient to affect adipogenesis. We also examined baseline differences in expression of a gene set previously identified using PPAR $\gamma^{-/-}$ cells reconstituted with viruses expressing WT or S273A PPAR γ (Choi et al., 2010). Surprisingly, expression of these genes was not significantly different in primary adipocytes differentiated *ex vivo* from WT and PPAR $\gamma^{A/A}$ mice (Figure S3C).

Given that PPAR γ S273 is phosphorylated in the setting of high-fat feeding (Choi et al., 2010), we maintained PPAR $\gamma^{A/A}$ and WT littermate mice on an HFD to promote obesity and insulin resistance. PPAR $\gamma^{A/A}$ and WT mice experienced equivalent weight gain (Figure 1A) with similar fat and lean body mass composition (Figure 1B). As PPAR γ activation with TZDs is associated with weight gain (Fonseca, 2003; Lu et al., 2011), we assessed energy balance by indirect calorimetry experiments in PPAR $\gamma^{A/A}$ mice. There were no significant differences observed for VO $_2$, VCO $_2$, calculated energy expenditure, food intake, body temperature, overall energy balance, locomotor activity, or ambulatory activity between genotypes (Figures S4A and S4B). We did observe a small but significant decrease in respiratory exchange ratio (RER) in the PPAR $\gamma^{A/A}$ animals, which is suggestive of increased fatty acid oxidation (Figure S4A).

We next assessed the effect of PPAR γ phosphorylation on glucose homeostasis in HFD-fed mice. Similar to effects observed in chow-fed mice, glucose tolerance was comparable between genotypes (Figures 1C and S2C). In contrast, insulin tolerance testing in HFD-fed mice revealed PPAR $\gamma^{A/A}$ mice to be more responsive to insulin, as evidenced by a significantly enhanced glucose lowering response (Figure 1D). To eliminate the possibility of pancreatic beta cell dysfunction, we assessed both fasting insulin levels and glucose-stimulated insulin levels in HFD-fed mice and found no difference between genotypes (Figures 1E and 1F). To better understand the insulin sensitivity phenotype, we performed hyperinsulinemic-euglycemic clamps on HFD-fed mice. We observed increases in the glucose infusion rate (GIR) required to maintain euglycemia in mutant mice compared to controls, indicating improved insulin sensitivity *per se* (Figure 1G). The primary factor contributing to the increased GIR is elevated whole-body glucose utilization, with pronounced effects observed in skeletal muscle, but not white adipose tissue (WAT) (Figures 1H–1J). Of note, there was no significant difference in the ability of insulin to suppress endogenous glucose production (EGP) (Figure 1K). These findings suggest that the improved insulin sensitivity is due to greater glucose uptake into tissues and is not due to decreased glucose production. The improved glucose uptake in muscle rather than fat is highly suggestive of tissue crosstalk. Importantly, we observed a 3-fold increase in the ability of insulin to suppress non-esterified fatty acid (NEFA) levels in PPAR $\gamma^{A/A}$ mice (Figure 1L).

We also examined biochemical indicators of insulin sensitivity and insulin signaling. PPAR $\gamma^{A/A}$ mice exhibited a modest but significant increase in insulin-stimulated AKT phosphorylation within skeletal muscle, but not liver, inguinal WAT (iWAT), or epididymal WAT (eWAT) (Figures 1M and 1N). These results strongly support the notion that phosphorylation of PPAR γ at S273 is sufficient to promote obesity-induced insulin resistance.

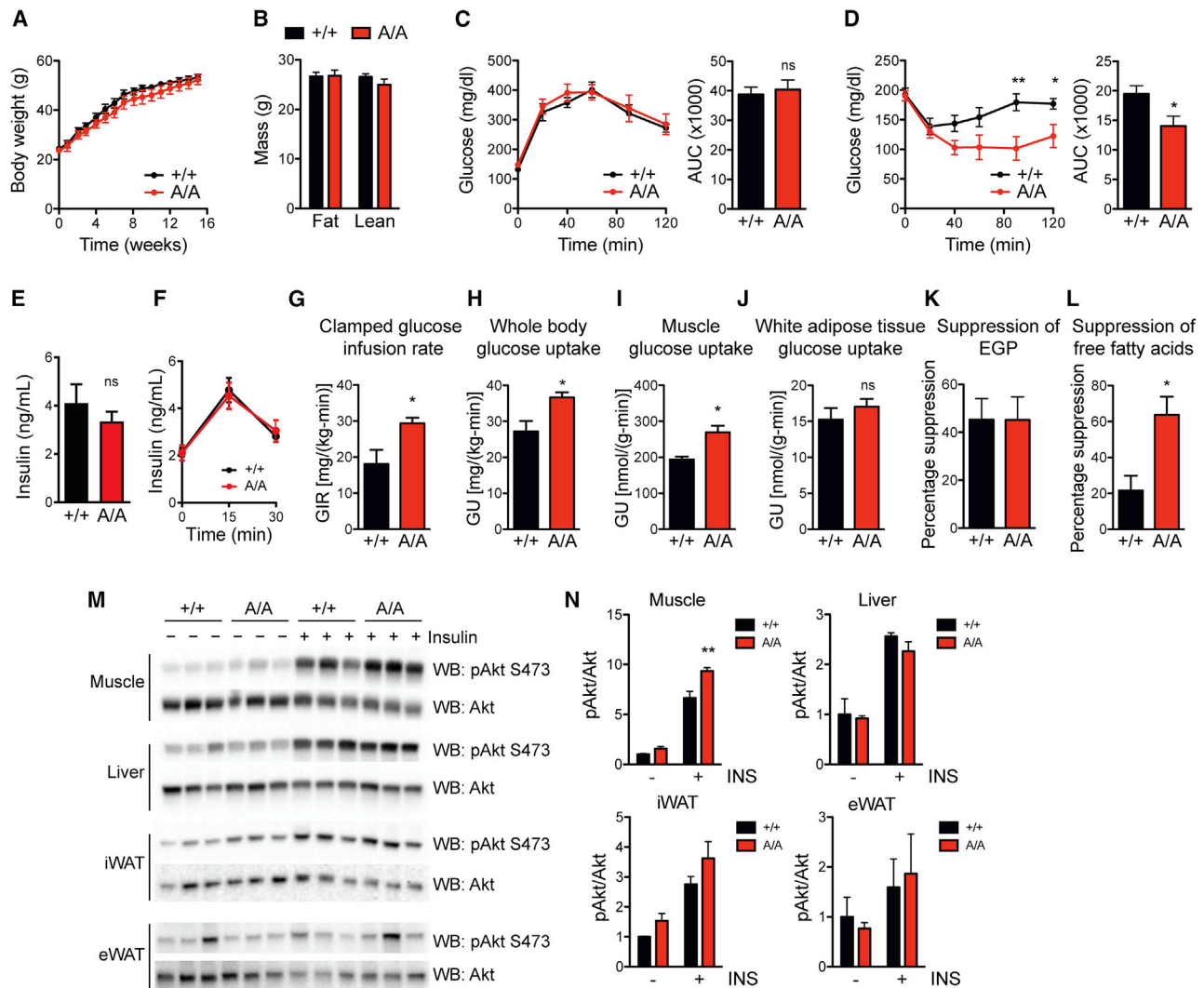


Figure 1. Improved Insulin Sensitivity in Mice with Non-phosphorylatable PPAR γ S273

Male WT (+/+) and PPAR $\gamma^{A/A}$ (A/A) mice were fed high-fat diet (HFD) for 16 weeks.

(A) Body weight of mice during HFD feeding (n = 6 +/+, 5 A/A).

(B) Body composition of mice at 16 weeks of HFD feeding, ns.

(C) Glucose tolerance test (1 g glucose/kg body weight) after 15 weeks on HFD.

(D) Insulin tolerance test (2 U insulin/kg body weight) after 16 weeks on HFD.

(C and D) Right: area under the curve (AUC) for the respective test. Results are representative of three independent experiments.

(E) Fasting insulin levels in male mice on HFD for 16 weeks and fasted overnight (n = 6 +/+, 5 A/A).

(F) Glucose (3 g glucose/kg body weight) stimulated insulin levels at indicated time points for male mice on HFD for 17 weeks (n = 6 +/+, 5 A/A).

(G–L) Hyperinsulinemic-euglycemic clamps in HFD-fed mice (n = 4 +/+, 5 A/A).

(G) Glucose infusion rate (GIR).

(H) Whole-body glucose uptake (GU).

(I) GU into skeletal muscle.

(J) GU into epididymal WAT.

(K) Percentage suppression of endogenous glucose production (EGP), ns.

(L) Percentage suppression of free fatty acids.

(M and N) Insulin sensitivity as determined by insulin-stimulated Akt phosphorylation (Ser 473) in tissues of HFD-fed +/+ and A/A mice.

(M) Immunoblot analyses of skeletal muscle, liver, inguinal WAT (iWAT), and epididymal WAT (eWAT).

(N) Quantification of blots in (M). Results are representative of at least two independent experiments.

Data are presented as mean \pm SEM; ns, not significant; *p < 0.05; **p < 0.01 by Student's t test (A–L) and one-way ANOVA with Newman-Keuls multiple comparison test (N).

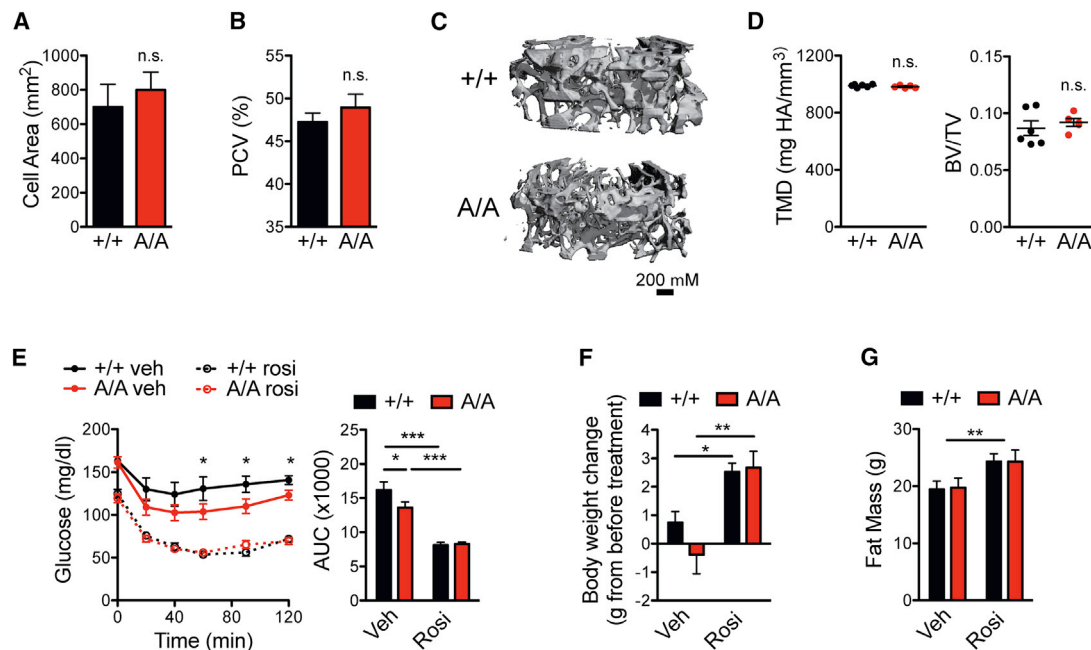


Figure 2. PPAR $\gamma^{A/A}$ and WT Mice Respond Similarly to PPAR γ Agonist Treatment

(A–D) PPAR $\gamma^{A/A}$ (A/A) mice fed HFD for 16 weeks do not innately exhibit the adverse effects associated with PPAR γ agonism.

(A) Average cell area of adipocytes from epididymal adipose tissue after HFD feeding (n = 3).

(B) Hematocrit (packed cell volume, PCV; n = 6 WT (+/+), 5 A/A).

(C and D) Microquantitative computed tomography (microCT) analysis of trabecular bone from femurs of 6-month-old mice maintained on HFD (n = 6 +/+, 5 A/A). (C) Representative image of microCT.

(D) Parameters from microCT analysis, including tissue mineral density (TMD, left) and trabecular bone volume fraction (BV/TV, right).

(E–G) Both +/+ and A/A mice respond to treatment with PPAR γ agonist rosiglitazone. After 19 weeks of HFD feeding, mice were treated with either vehicle or rosiglitazone (rosi) for 10 days (8 mg/kg body weight; n = 7 per genotype).

(E) Insulin tolerance test (1.5 U insulin/kg body weight); right, area under the curve (AUC).

(F) Body weight gained over course of treatment.

(G) Total fat mass at end of treatment.

Data are presented as mean \pm SEM; *p < 0.05; **p < 0.01; ***p < 0.001 by one-way ANOVA with Newman-Keuls multiple comparison (E and F) and two-way ANOVA (G).

PPAR $\gamma^{A/A}$ and WT Mice Respond Similarly to PPAR γ Agonist Treatment

The TZD class of insulin sensitizing drugs serves both as agonists and to prevent phosphorylation of PPAR γ S273. However, these drugs also have adverse effects, such as weight gain, fluid retention, and bone loss (Chilcott et al., 2001). Whether these side effects are completely separable from insulin sensitization is a key unanswered question. Multiple small-molecule non-agonist ligands have successfully separated beneficial from adverse effects (Amato et al., 2012; Choi et al., 2014; Stechschulte et al., 2016). To test whether this phenomenon holds true in a genetic model, we assessed PPAR $\gamma^{A/A}$ mice for TZD-associated side effects. First, adipocytes in eWAT of PPAR $\gamma^{A/A}$ mice had similar cell surface area to cells from control mice (Figure 2A). In addition, PPAR $\gamma^{A/A}$ mice fed HFD showed no decrease in hematocrit, as an indicator of fluid retention (Figure 2B), compared to controls. Importantly, using microquantitative computed tomography (microCT), we also observed no change in tissue mineral density (TMD) or trabecular bone volume fraction among genotypes (Figures 2C and 2D). Cortical bone parameters, including thickness, mineralization, and periosteal perimeter, were similarly unchanged (data not shown).

Thus, while mice harboring the S273A knockin allele recapitulate the PPAR γ agonist-like improvements in insulin sensitivity, they avoid the adverse effects typically associated with TZDs. Treatment of HFD-fed PPAR $\gamma^{A/A}$ mice with the full agonist of PPAR γ , rosiglitazone, revealed a further improvement in insulin sensitivity (Figure 2E). These effects included the adverse effects, weight gain and increased adiposity (Figures 2F and 2G). These results indicate that while PPAR $\gamma^{A/A}$ mice show an improvement in glucose homeostasis, these animals are still susceptible to certain beneficial effects of TZD treatment and to the full adverse effects of these drugs.

Expression of Gdf3 Is Associated with PPAR γ S273 Phosphorylation

As PPAR γ is phosphorylated in obese states and is highly expressed in adipose tissue, we examined transcriptional differences between control and littermate PPAR $\gamma^{A/A}$ eWAT from mice on HFD. Differential gene expression analysis following RNA sequencing (RNA-seq) in eWAT revealed one striking result in the mutant animals: a strong and significant ($p < 10^{-12}$) down-regulation of Gdf3, a secreted protein and member of the TGF- β superfamily (Figure 3A). Using qPCR, we confirmed Gdf3 was

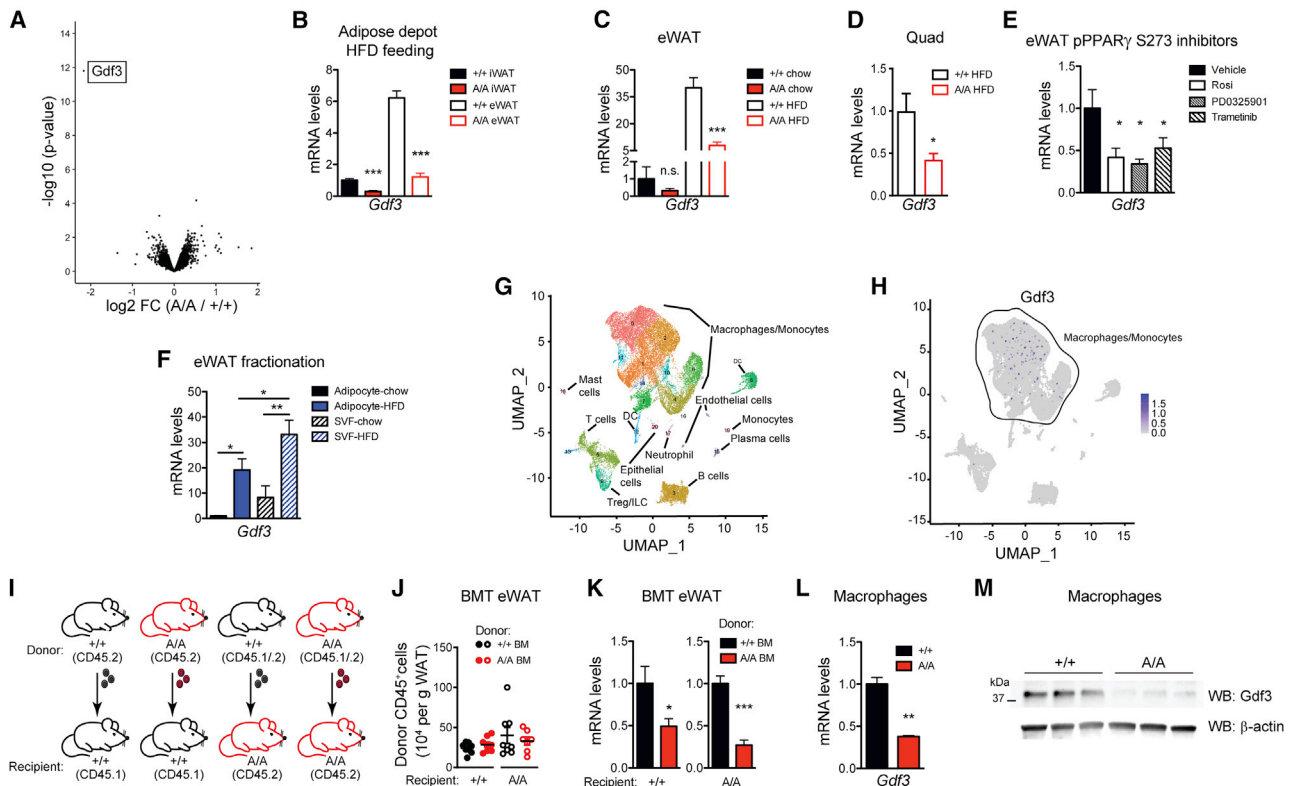


Figure 3. Expression of *Gdf3* Is Associated with PPAR γ S273 Phosphorylation

(A and B) PPAR $\gamma^{A/A}$ (A/A) and wildtype (+/+) mice fed HFD for 37 weeks.

(A) Volcano plot from RNA-seq analysis on eWAT, with differentially expressed gene *Gdf3* highlighted.

(B) qPCR validation of decreased *Gdf3* mRNA levels in eWAT and iWAT of HFD-fed A/A mice.

(C) *Gdf3* mRNA levels in eWAT from mice on chow or HFD for 25 weeks.

(D) *Gdf3* mRNA levels in quadriceps from mice fed HFD for 17 weeks.

(E) *Gdf3* mRNA levels in obese adipose tissue also decrease following treatment with known inhibitors of PPAR γ S273 phosphorylation (rosiglitazone or either of two MEK inhibitors, PD0325901 or Trametinib; n = 4–6).

(F) Fractionated adipose tissue indicates *Gdf3* is highly expressed in both the SVF and adipocyte fractions of eWAT from mice fed HFD for 10 weeks.

(G and H) Single-cell RNA-seq of SVF from HFD-fed +/+ mice shows detectable expression mainly in the macrophage/monocyte population.

(I–K) Generation of bone marrow chimeras reveals dominant role of hematopoietic cells in decreased *Gdf3* expression of A/A mice.

(l) Scheme used for bone marrow transplantation study, including use of congenic C57BL/6 strains carrying functionally equivalent alleles of the pan leukocyte marker CD45.

(J) Quantification of donor CD45 $^{+}$ cells in recipient eWAT tissue after HFD treatment of chimeric mice (n = 7–8).

(K) *Gdf3* mRNA levels in eWAT after HFD treatment of chimeric mice (n = 7–8).

(L and M) Thioglycollate-elicited peritoneal macrophages from chow-fed A/A mice exhibit decreased *Gdf3* (L) mRNA and (M) protein levels.

Data are presented as mean \pm SEM; *p < 0.05; **p < 0.01; ***p < 0.001 by Student's t test (B–D, per tissue/condition; J–L) and one-way ANOVA with Newman-Keuls multiple comparison test (E and F).

expressed at lower levels in both PPAR $\gamma^{A/A}$ iWAT and eWAT from HFD-fed mice when compared to littermate controls (Figure 3B). Consistent with previously published data, eWAT *Gdf3* levels increase in obesity (Wang et al., 2004). *Gdf3* expression shows a 35-fold increase in the eWAT of WT mice maintained on HFD for 25 weeks compared to chow-fed controls. In contrast, the induction of *Gdf3* by HFD was reduced 80% in the eWAT of PPAR $\gamma^{A/A}$ mice. No significant difference was observed between genotypes on a standard chow diet (Figure 3C). We also saw a significant decrease in *Gdf3* mRNA levels in the skeletal muscle (quadriceps) of HFD-fed PPAR $\gamma^{A/A}$ mice (Figure 3D). We next investigated *Gdf3* regulation by non-genetic modulation of PPAR γ S273 phosphorylation using small molecules that can limit S273 phosphorylation of PPAR γ . Mice

were treated with rosiglitazone, a PPAR γ agonist, or with MEK inhibitors, GSK1120212 (Trametinib) or PD0325901, to reduce PPAR γ phosphorylation. *Gdf3* mRNA levels decreased significantly in eWAT of these mice in response to rosiglitazone, Trametinib, and PD0325901 by 60%, 68%, and 50%, respectively (Figure 3E).

***Gdf3* Is Most Highly Expressed in Adipose Tissue Macrophages from HFD Mice**

Due to the heterogeneous composition of adipose tissue, we examined whether *Gdf3* levels were found within a population of fractionated adipocytes or the stromal vascular fraction (SVF). Although HFD treatment increased *Gdf3* expression in both adipocyte and SVFs, higher *Gdf3* mRNA levels were

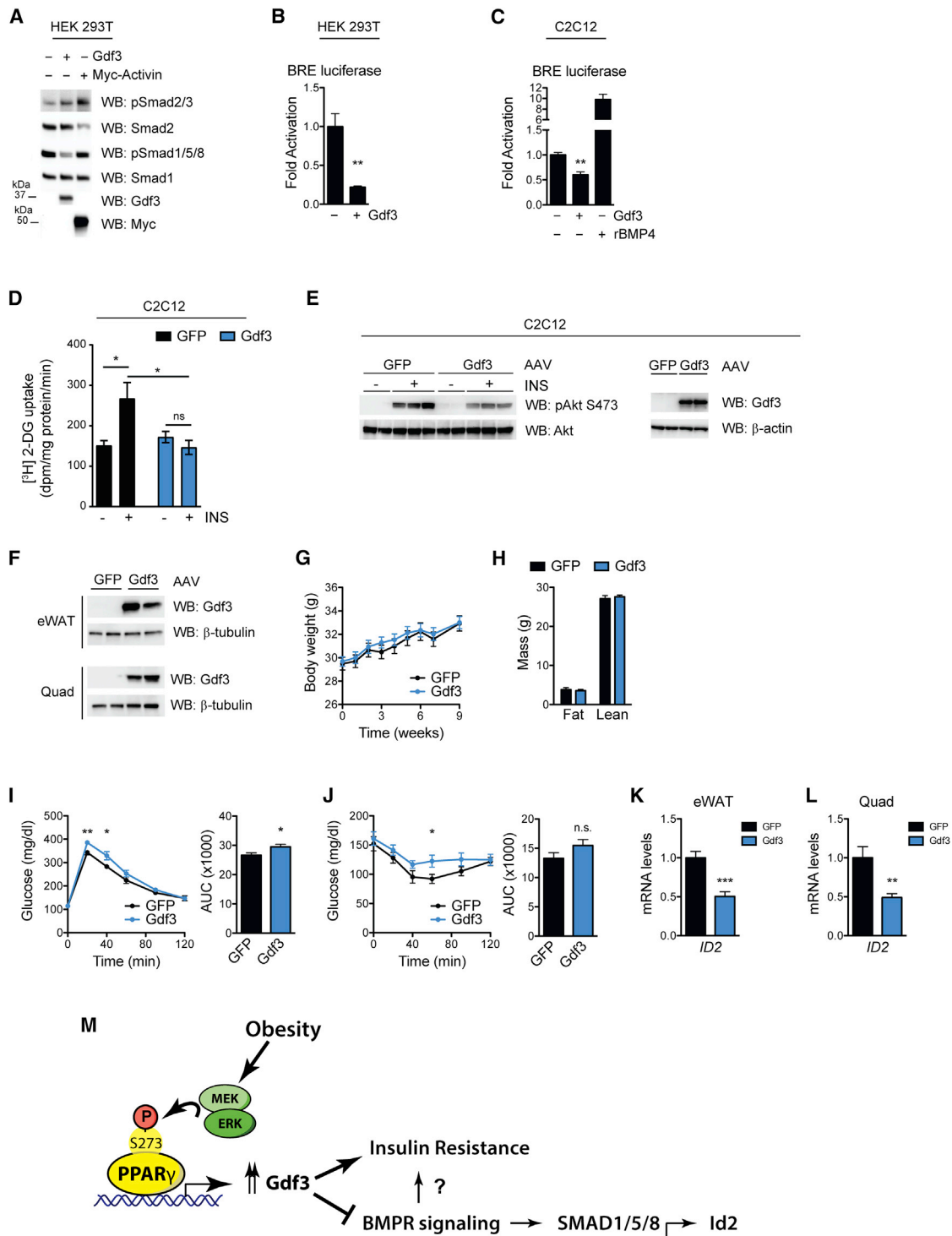


Figure 4. GDF3 Limits BMP Signaling, Affects Glucose Uptake *In Vitro*, and Is Sufficient to Induce Insulin Resistance *In Vivo*

(A) Immunoblot analysis of HEK293T cells transfected with Gdf3 or Myc-Activin constructs. Cells were deprived of serum for 16 h prior to whole-cell extract. (B) Luciferase assay using a BMP-responsive element (BRE) driving luciferase reporters in serum-starved HEK293T cells.

(C) BRE luciferase assay in C2C12 myoblasts that have been deprived of serum. Overnight treatment of 100 ng/mL rBMP4 demonstrates reporter activation.

(D and E) C2C12 myotubes transduced with AAV-GFP or AAV-Gdf3.

(D) [³H] 2-deoxy-D-glucose (2-DG) uptake assays, n = 6 wells per group.

(E) Immunoblot analyses.

(F–L) As a gain-of function model, 13-week-old male mice were administered AAV-GFP or AAV-Gdf3, n = 10 mice per group.

(legend continued on next page)

observed in the SVF (Figure 3F). Single-cell RNA-seq of mouse SVF from HFD-fed mice (Jaitin et al., 2019) suggests that Gdf3 is localized to macrophage/monocyte cells within the SVF (Figures 3G and 3H). To assess the contribution of macrophage-specific PPAR γ S273 phosphorylation to obesogenic Gdf3 expression, we generated bone marrow chimeras and asked whether obese WT mice with a PPAR $\gamma^{A/A}$ immune system will have altered Gdf3 expression (Figure 3I). We found no differences in numbers of CD45 $^{+}$ cells infiltrating recipient eWAT, irrespective of the donor genotype (Figure 3J). Strikingly, mice with a hematopoietic compartment reconstituted from PPAR $\gamma^{A/A}$ donors exhibited lower Gdf3 expression in eWAT regardless of recipient genotype (Figure 3K). Thus, transplantation with PPAR $\gamma^{A/A}$ bone marrow recapitulated the decreased Gdf3 levels observed with whole-body PPAR $\gamma^{A/A}$ animals. Moreover, peritoneal macrophages from PPAR $\gamma^{A/A}$ mice revealed a 65% reduction in the levels of Gdf3 mRNA and an 80% reduction in protein levels (Figures 3L and 3M). Together, these data provide strong evidence for the regulation of Gdf3 by PPAR γ S273 phosphorylation.

To further determine whether the differential levels of Gdf3 levels in adipose tissue were due to decreased numbers of Gdf3-expressing cells or to specific modulation of gene expression, we performed detailed immunophenotyping on eWAT from WT and PPAR $\gamma^{A/A}$ mice maintained on HFD for 16 weeks. None of the macrophage or T cell populations examined showed significant differences when either the cell number or the percentage of gated cells was examined between genotypes. Macrophage populations were gated according to the strategy outlined in Figure S5A. No differences were observed in total macrophage number or percent of gated live, hematopoietic cells (CD45 $^{+}$) that were not eosinophils (Siglec F $^{-}$) (Figure S5B). Nor were differences in macrophage percent of cells expressing an M1 marker (CD11c $^{+}$) or an M2 marker (CD301 $^{+}$) (Figure S5C). PPAR γ is highly expressed in T regulatory cells (Tregs), a cell type that can control tissue inflammation including macrophage recruitment (Cipolletta et al., 2012, 2015). Treg populations were gated according to the strategy outlined in Figure S5D. No differences were observed in total Treg number or percent of gated live, hematopoietic cells (CD45 $^{+}$) that expressed the T cell receptor, CD4 co-receptor, and transcription factor Foxp3 (TCRb $^{+}$ CD4 $^{+}$ Foxp3 $^{+}$) (Figure S5E). Similarly, tissue-resident Tregs (KLRG1 $^{+}$ ST2 $^{+}$) had no significant differences (Figure S5F). Coupled with the lack of cell-type-specific gene regulation, these data support the conclusion that similar levels of hematopoietic cells are present in PPAR $\gamma^{A/A}$ adipose tissue. These findings strongly suggest the differences in Gdf3 expression levels in PPAR $\gamma^{A/A}$ adipose tissue reflect specific transcriptional control by PPAR γ S273 phosphorylation.

GDF3 Limits BMP Signaling

Members of the TGF- β superfamily, including BMPs, GDFs, and TGF- β proteins, can affect insulin sensitivity, cellular differentiation, and obesity (Chattopadhyay et al., 2017; Chen et al., 2003; Pauk et al., 2019; Schreiber et al., 2017). These proteins typically work either through BMP-type receptors or TGF- β -type receptors. Relatively little is known of mammalian Gdf3 function on glucose homeostasis *in vivo*. Two seemingly incompatible models have been proposed to explain how extracellular Gdf3 signaling is propagated. One model suggests that Gdf3 can inhibit BMP-receptor signaling, possibly by competing with other ligands for receptor binding (Levine and Brivanlou, 2006; Levine et al., 2009). In the other model, Gdf3 activates TGF- β -type receptors (ALK7/Cripto), especially at super-physiological concentrations of 300–500 ng/mL (Andersson et al., 2008; Bu et al., 2018; Chen et al., 2006). We examined whether Gdf3 can affect either signaling system using a WT full-length Gdf3 cDNA expressed in human HEK293T cells. As reported previously, Activin, a TGF- β receptor ligand, activates Smad2/3 phosphorylation. In contrast, Gdf3 had little impact on TGF- β signaling. Activin neither promotes nor inhibits BMP-receptor signaling as measured by phosphorylation of SMAD1/5/8. However, cells expressing Gdf3 demonstrate a strong reduction of SMAD1/5/8 phosphorylation (Figure 4A).

To understand the integrated effects of Gdf3 over time, we performed luciferase reporter assays to quantify Gdf3 transcriptional consequences. In these reporter assays, BMP signaling promotes SMAD 1/5/8 binding to the BMP responsive element (BRE) of the Id1 promoter. We observed an 80% reduction of luciferase activity with Gdf3 overexpression compared to control cells expressing an empty vector (Figure 4B). We further confirmed these results in a second cell type, C2C12 myoblasts. As in HEK293T cells, Gdf3 decreases BRE-Luc by 50% compared to control cells. As a positive control, recombinant BMP4 activates BMP receptor signaling and stimulates Smad1/5/8 activity (Figure 4C). These data suggest that Gdf3 is a BMP inhibitor in a class similar to Noggin or Gremlin (Daluisi et al., 2001; Lim et al., 2000).

GDF3 Affects Glucose Uptake In Vitro

Based on the increased skeletal muscle glucose uptake in HFD-fed PPAR $\gamma^{A/A}$ mice, and the luciferase reporter assay in C2C12 myoblasts, we wanted to determine if regulating GDF3 levels in muscle cells could affect insulin-dependent glucose uptake. To test this, we transduced differentiated C2C12 myotubes with either an adeno-associated virus (AAV) expressing GFP (AAV-GFP) or an AAV expressing Gdf3 (AAV-Gdf3). GDF3 overexpression in these cells led to decreased glucose uptake in the presence of insulin, compared to GFP-expressing cells. No

(F) Immunoblots from eWAT and quadriceps from two mice from each group, 9 weeks post-injections.

(G) Body weights of mice; week 0 represents the values on the day of AAV injections.

(H) Body composition at 6 weeks post-injections.

(I) Glucose tolerance test (2 g glucose/kg body weight) 4 weeks post-injections. Right: area under the curve (AUC).

(J) Insulin tolerance test (0.75 U insulin/kg body weight) 3 weeks post-injections. Right: area under the curve (AUC).

(K and L) Relative Id2 mRNA levels from eWAT (K) and quadriceps (L).

(M) Model illustrating novel role for PPAR γ S273 phosphorylation and Gdf3 in impaired insulin action with obesity.

Data are presented as relative activity after normalization to Renilla luciferase (B and C) and as mean \pm SEM (B–D and G–L); ns, not significant; *p < 0.05; **p < 0.01; ***p < 0.001 by Student's t test (B, C, and G–L) and two-way ANOVA with Sidak's multiple comparison test (D).

differences between groups were observed under baseline (no insulin) (Figure 4D). Immunoblot analyses of these cells under similar conditions revealed a decrease in insulin-stimulated AKT phosphorylation in GDF3-overexpressing cells (Figure 4E). Together, these results suggest that GDF3 overexpression is sufficient to inhibit glucose uptake and reduce insulin signaling in muscle cells *in vitro*.

GDF3 Is Sufficient to Induce Insulin Resistance *In Vivo*

To investigate the effect of GDF3 *in vivo*, we administered AAV-GFP or Gdf3 into the visceral fat pads (eWAT) and skeletal muscles (quadriceps and gastrocnemius) of lean WT mice, resulting in a detectable increase in protein levels of Gdf3 (Figure 4F). Forced GDF3 expression did not affect body weight, body composition, energy expenditure, or food intake of mice fed a chow diet (Figures 4G and 4H; data not shown). Importantly, mice overexpressing GDF3 had impairments in both glucose tolerance and insulin tolerance tests (Figures 4I and 4J). These data indicate that increased levels of GDF3 in these tissues are sufficient to negatively impact glucose homeostasis, independently of changes in body weight. The inhibitors of differentiation (Id) genes, including *Id2*, are canonical targets of BMPR signaling (Izumi et al., 2006). We examined the effect of AAV Gdf3 expression on *Id2* mRNA levels in eWAT and quadriceps. In both tissues, we observed significant downregulation (Figures 4K and 4L), consistent with inhibition of BMPR signaling *in vivo*. These effects of GDF3 to promote impaired glucose homeostasis in healthy, lean mice suggest that the elevated GDF3 levels observed in obesity may contribute to insulin resistance.

DISCUSSION

The link between PPAR γ biology and insulin sensitivity is both robust and complex. Patients treated with TZD PPAR γ agonists experience durable reduced glycemia and insulin sensitivity. These effects were long thought to depend on PPAR γ -driven adipogenesis—the generation of new, healthy adipocytes from precursor cells. The properties of PPAR γ agonists to promote adipocyte differentiation cause weight gain, but also decrease bone formation, leading to increased risk of fractures. The demonstration that blocking PPAR γ S273 phosphorylation can improve insulin sensitivity independently of receptor agonism or effects on bone suggests new therapeutic approaches to insulin sensitizers.

Increased PPAR γ S273 phosphorylation induced by ERK kinase in obesity contributes to insulin resistance. Our study shows that preventing S273 phosphorylation genetically was sufficient to maintain insulin sensitivity in obesity, as manifested by improved insulin tolerance and increased whole-body glucose utilization (Figure 1). Consistent with this interpretation, in lean WT chow-fed mice in which the receptor was not phosphorylated, we did not observe differences in glucose homeostasis from littermate PPAR $\gamma^{A/A}$ mice. (Figure S2). This suggests that the observed phenotypic changes were due to the contribution of obesity, rather than developmental effects. Moreover, as PPAR γ S273 phosphorylation is independent of receptor agonism, we did not observe TZD-like side effects in PPAR $\gamma^{A/A}$ mice (Figure 2). Interestingly, our insulin-sensitive phenotype in PPAR $\gamma^{A/A}$ mice was not accompanied by increased glucose

tolerance or changes in insulin secretion. The hyperinsulinemic-euglycemic clamp experiment also showed increased muscle glucose uptake in PPAR $\gamma^{A/A}$ mice with no significant changes in adipose glucose uptake or insulin-dependent suppression of endogenous glucose production. Together these results were unexpected but seem to indicate that the effects of suppression of PPAR γ S273 phosphorylation might affect only a subset of PPAR γ -expressing tissues.

Differentiated primary adipocytes from WT and PPAR $\gamma^{A/A}$ mice did not show differences in the expression of a previously established gene set regulated by PPAR γ S273 phosphorylation. This lack of differential gene expression could be related to the absence of ERK signaling or inflammation in our experimental conditions, environments that promote PPAR γ S273 phosphorylation. Alternatively, this could be due to the difference between a chronic genetic mutation and acute treatments of PPAR γ agonists or retroviral PPAR $\gamma^{A/A}$ expression (Choi et al., 2010; Figure S3).

We identified Gdf3 as a transcriptional target of PPAR γ S273 phosphorylation in obese adipose tissue as well as skeletal muscle. Gdf3 was expressed in adipose tissue in both the SVF and adipocyte fractions, with highest levels observed in macrophages (Figure 3). We also show that bone marrow-derived macrophages transplanted from PPAR $\gamma^{A/A}$ mice can lead to lower Gdf3 expression in the adipose tissue of recipient mice, and WT macrophages could rescue Gdf3 levels in PPAR $\gamma^{A/A}$ recipients (Figure 3). Previous studies of macrophage-specific PPAR γ deficiency identified strongly reduced Gdf3 mRNA levels in the absence of PPAR γ , along with the binding of PPAR γ and RXR to potential enhancer regions of the Gdf3 locus (Varga et al., 2016). While macrophage PPAR γ -deficient mice expressed low Gdf3 levels, which would predict insulin sensitivity, they nonetheless exhibited insulin resistance due to increased secretion of multiple pro-inflammatory cytokines (Chawla et al., 2001; Hevener et al., 2007; Morán-Salvador et al., 2011; Odegaard et al., 2007; Varga et al., 2016). In contrast, PPAR $\gamma^{A/A}$ mice did not have significant differences in macrophage number, relative polarization, or cytokine expression levels (Figure S5).

Relatively little is known of mammalian Gdf3 function on glucose homeostasis *in vivo*. Gdf3 is highly expressed in WAT with levels increasing with age and obesity (Bu et al., 2018; Camell et al., 2017; Wang et al., 2004). Our *in vitro* studies in C2C12 myotubes with AAV-mediated Gdf3 expression showed that Gdf3 was sufficient to reduce insulin signaling and insulin-mediated glucose uptake in muscle cells (Figures 4D and 4E). Although cells in culture cannot be directly extrapolated to *in vivo* functions, we also saw from our *in vivo* AAV-mediated Gdf3 expression in the eWAT and skeletal muscle of mice that Gdf3 overexpression was sufficient to cause insulin resistance and glucose intolerance in chow-fed lean mice (Figures 4F, 4I, and 4J). The mechanisms of these effects are still unclear, but our data support a model in which Gdf3 blocks beneficial BMPR signaling, decreasing phosphorylation of SMAD 1/5/8 and inhibiting *Id2*, a SMAD target gene (Figure 4).

Our work is consistent with studies demonstrating improvements in glucose homeostasis by increasing levels of BMP4 or BMP signaling. Conversely, BMP4 knockout mice exhibit impaired glucose tolerance (Hoffmann et al., 2017; Qian et al.,

2013). Heterozygous deletion of the type 1 BMP receptor, *Bmpr1a*, causes impaired glucose tolerance (Scott et al., 2009), while adipocyte-specific receptor deletion does not (Schulz et al., 2016). Similar salutary effects of glucose homeostasis have been observed in mice treated with BMP6, BMP7, and BMP9 (Chattopadhyay et al., 2017; Chen et al., 2003; Pauk et al., 2019). BMPs can drive cellular differentiation including potentiation of brown and beige fat activation (Hoffmann et al., 2017; Qian et al., 2013; Schulz et al., 2013). In this context, tight control of BMP signaling is maintained by inhibitory proteins including Gdf3, Noggin, and Gremlin (Hsu et al., 1998; Levine and Brivanlou, 2006).

An emerging literature is developing on the contribution of macrophages to catecholamine production and degradation. Macrophages expressing Gdf3 have been implicated in controlling catecholamine degradation and rates of lipolysis (Camell et al., 2017). Mice with global deletion of Gdf3 from birth maintain lean body masses when challenged with HFD (Andersson et al., 2008; Shen et al., 2009). Conversely, Gdf3 has been reported to induce severe and persistent obesity in an adenovirus overexpression model in response to HFD feeding (Wang et al., 2004). We observed no differences in energy balance compared to control mice in our models of decreased Gdf3 levels (PPAR γ ^{AA} mice) when challenged with HFD or with exogenous Gdf3 expression using AAV under chow-fed conditions (Figure 4). These differences may be due to the role of Gdf3 in embryonic development (Chen et al., 2006; Levine and Brivanlou, 2006) versus the late timing of Gdf3 expression changes driven by differential obesity-mediated phosphorylation of PPAR γ S273 or also on the late timing and tissue specificity of AAV-mediated Gdf3 expression.

Future studies will determine whether Gdf3 inhibits BMP-receptor signaling by binding to the BMP receptor or through inhibitory binding to other extracellular BMP receptor ligands and if these interactions are sufficient to cause the insulin resistance phenotype of Gdf3 overexpression. We find that Gdf3 is a factor that mediates the adverse consequences of obesity-mediated PPAR γ S273 phosphorylation. Further study into the mechanisms of Gdf3 action will be beneficial to understand whether this is an appropriate future therapeutic target.

Limitations of Study

While our study demonstrates a causal role for PPAR γ S273 phosphorylation in insulin resistance, the use of a whole-body knockin model does not allow us identification of primary tissues driving this effect. In addition, although Gdf3 has previously been identified as a PPAR γ target gene, our study does not show a direct mechanism for how PPAR γ S273 phosphorylation alters Gdf3 expression, nor why the regulation of this gene is so selective. We demonstrate that Gdf3 levels correlate with insulin resistance, yet we do not have an elucidated mechanism to understand how Gdf3 promotes the development of insulin resistance. These efforts are needed as considerable controversy exists addressing many of the fundamental questions of Gdf3 biology including dimerization partners, receptor identity, and signaling cascade. Our data indicate macrophages are likely to be the primary source of the elevated Gdf3 levels induced with obesity; however, further studies are required to confirm this finding.

STAR★METHODS

Detailed methods are provided in the online version of this paper and include the following:

- KEY RESOURCES TABLE
- RESOURCE AVAILABILITY
 - Lead Contact
 - Materials Availability
 - Data and Code Availability
- EXPERIMENTAL MODEL AND SUBJECT DETAILS
 - Mouse Model
 - Cell Lines
 - Primary Cell Culture
- METHOD DETAILS
 - Animal Experiments
 - *In Vivo* AAV Experiments
 - Glucose and Insulin Tolerance Tests
 - Hyperinsulinemic-Euglycemic Clamp
 - Indirect Calorimetry
 - Microquantitative Computed Tomography
 - RNA Isolation and Gene Expression Analysis by qPCR, RNA-seq, or Single Cell RNA-seq
 - Preparation of Cell or Tissue Lysates and Immunoblotting
 - DNA Constructs and AAVs
 - Lipid Accumulation Assay
 - Glucose Uptake Assays
 - Luciferase Reporter Assays
 - Isolation of Macrophages
 - Isolation of Cells from SVF
 - Immunophenotyping and Flow Cytometry
 - Bone Marrow Transplantation
- QUANTIFICATION AND STATISTICAL ANALYSIS

SUPPLEMENTAL INFORMATION

Supplemental Information can be found online at <https://doi.org/10.1016/j.cmet.2020.08.016>.

ACKNOWLEDGMENTS

Animal assistance was provided by Yuchen He and June Corrigan. Financial support for this project was provided from the NIH to A.S.B.: R01DK107717, P30DK34854, and U24DK076169 for the NIDDK Mouse Metabolic Phenotyping Centers under the MICROMouse Program. J.A.H. received support from the NIH T32DK007529-28. D.R. was supported by the Swiss National Science Foundation's Early Postdoc Mobility grant. E.D.R. was supported by NIH R01 DK102173 and DK113669. T.B. was supported by the São Paulo Research Foundation (postdoc financial support #2017/25881-0). RNA-seq was performed by the Boston Nutrition and Obesity Research Center's Functional Genomics and Bioinformatics Core (BNORC, NIH 5P30DK046200).

AUTHOR CONTRIBUTIONS

Conceptualization, J.A.H., D.R., B.M.S., and A.S.B.; Methodology, J.A.H., D.R., and A.S.B.; Investigation, J.A.H., D.R., A.S.B., H.C.R., J.R.D., T.B., L.T.Y.T., D.T., P.-J.H.Z., C.P., S.H., A.I.M., B.L., Z.D., P.A., and J.F.C.; Software, A.S.B., C.J., and L.T.Y.T.; Resources, C.W.B., G.I.S., B.B.K., E.D.R., and B.M.S.; Formal Analysis, J.A.H., D.R., and A.S.B.; Data Curation, A.S.B.; Writing – Original Draft, J.A.H., D.R., and A.S.B.; Writing – Review & Editing, J.A.H., D.R., and A.S.B.; Visualization, J.A.H., D.R., and A.S.B.; Funding Acquisition and Supervision, B.M.S. and A.S.B.

DECLARATION OF INTERESTS

E.D.R. is a paid consultant of Novartis. B.B.K. consults for Alterna and serves on the Scientific Advisory Board of Janssen Pharmaceuticals. A.S.B. and B.M.S. hold a patent related to this work.

Received: January 23, 2020

Revised: June 5, 2020

Accepted: August 26, 2020

Published: September 16, 2020

REFERENCES

- Altshuler, D., Hirschhorn, J.N., Klannemark, M., Lindgren, C.M., Vohl, M.C., Nemesh, J., Lane, C.R., Schaffner, S.F., Bolk, S., Brewer, C., et al. (2000). The common PPAR γ Pro12Ala polymorphism is associated with decreased risk of type 2 diabetes. *Nat. Genet.* 26, 76–80.
- Amato, A.A., Rajagopalan, S., Lin, J.Z., Carvalho, B.M., Figueira, A.C., Lu, J., Ayers, S.D., Mottin, M., Silveira, R.L., Souza, P.C., et al. (2012). GQ-16, a novel peroxisome proliferator-activated receptor γ (PPAR γ) ligand, promotes insulin sensitization without weight gain. *J. Biol. Chem.* 287, 28169–28179.
- Andersson, O., Korach-Andre, M., Reissmann, E., Ibáñez, C.F., and Bertolino, P. (2008). Growth/differentiation factor 3 signals through ALK7 and regulates accumulation of adipose tissue and diet-induced obesity. *Proc. Natl. Acad. Sci. USA* 105, 7252–7256.
- Banks, A.S., McAllister, F.E., Camporez, J.P., Zushin, P.J., Jurczak, M.J., Laznik-Bogoslavski, D., Shulman, G.I., Gygi, S.P., and Spiegelman, B.M. (2015). An ERK/Cdk5 axis controls the diabetogenic actions of PPAR γ . *Nature* 517, 391–395.
- Boden, G. (1997). Role of fatty acids in the pathogenesis of insulin resistance and NIDDM. *Diabetes* 46, 3–10.
- Bouhler, M.A., Derudas, B., Rigamonti, E., Diévert, R., Brozek, J., Haulon, S., Zawadzki, C., Jude, B., Torpier, G., Marx, N., et al. (2007). PPAR γ activation primes human monocytes into alternative M2 macrophages with anti-inflammatory properties. *Cell Metab.* 6, 137–143.
- Bouxsein, M.L., Boyd, S.K., Christiansen, B.A., Guldberg, R.E., Jepsen, K.J., and Müller, R. (2010). Guidelines for assessment of bone microstructure in rodents using micro-computed tomography. *J. Bone Miner. Res.* 25, 1468–1486.
- Bu, Y., Okunishi, K., Yogosawa, S., Mizuno, K., Irudayam, M.J., Brown, C.W., and Izumi, T. (2018). Insulin regulates lipolysis and fat mass by upregulating growth/differentiation factor 3 in adipose tissue macrophages. *Diabetes* 67, 1761–1772.
- Camell, C.D., Sander, J., Spadaro, O., Lee, A., Nguyen, K.Y., Wing, A., Goldberg, E.L., Youm, Y.H., Brown, C.W., Elsworth, J., et al. (2017). Inflammation-driven catecholamine catabolism in macrophages blunts lipolysis during ageing. *Nature* 550, 119–123.
- Chattopadhyay, T., Singh, R.R., Gupta, S., and Suroli, A. (2017). Bone morphogenetic protein-7 (BMP-7) augments insulin sensitivity in mice with type II diabetes mellitus by potentiating PI3K/AKT pathway. *Biofactors* 43, 195–209.
- Chawla, A., Barak, Y., Nagy, L., Liao, D., Tontonoz, P., and Evans, R.M. (2001). PPAR- γ dependent and independent effects on macrophage-gene expression in lipid metabolism and inflammation. *Nat. Med.* 7, 48–52.
- Chen, C., Grzegorzewski, K.J., Barash, S., Zhao, Q., Schneider, H., Wang, Q., Singh, M., Pukac, L., Bell, A.C., Duan, R., et al. (2003). An integrated functional genomics screening program reveals a role for BMP-9 in glucose homeostasis. *Nat. Biotechnol.* 21, 294–301.
- Chen, C., Ware, S.M., Sato, A., Houston-Hawkins, D.E., Habas, R., Matzuk, M.M., Shen, M.M., and Brown, C.W. (2006). The Vg1-related protein Gdf3 acts in a Nodal signaling pathway in the pre-gastrulation mouse embryo. *Development* 133, 319–329.
- Chilcott, J., Tappenden, P., Jones, M.L., and Wight, J.P. (2001). A systematic review of the clinical effectiveness of pioglitazone in the treatment of type 2 diabetes mellitus. *Clin. Ther.* 23, 1792–1823, discussion 1791.
- Choi, J.H., Banks, A.S., Estall, J.L., Kajimura, S., Boström, P., Laznik, D., Ruas, J.L., Chalmers, M.J., Kamenecka, T.M., Blüher, M., et al. (2010). Anti-diabetic drugs inhibit obesity-linked phosphorylation of PPAR γ by Cdk5. *Nature* 466, 451–456.
- Choi, J.H., Banks, A.S., Kamenecka, T.M., Busby, S.A., Chalmers, M.J., Kumar, N., Kuruvilla, D.S., Shin, Y., He, Y., Bruning, J.B., et al. (2011). Antidiabetic actions of a non-agonist PPAR γ ligand blocking Cdk5-mediated phosphorylation. *Nature* 477, 477–481.
- Choi, S.S., Kim, E.S., Koh, M., Lee, S.J., Lim, D., Yang, Y.R., Jang, H.J., Seo, K.A., Min, S.H., Lee, I.H., et al. (2014). A novel non-agonist peroxisome proliferator-activated receptor γ (PPAR γ) ligand UHC1 blocks PPAR γ phosphorylation by cyclin-dependent kinase 5 (CDK5) and improves insulin sensitivity. *J. Biol. Chem.* 289, 26618–26629.
- Cipolletta, D., Feuerer, M., Li, A., Kamei, N., Lee, J., Shoelson, S.E., Benoist, C., and Mathis, D. (2012). PPAR- γ is a major driver of the accumulation and phenotype of adipose tissue Treg cells. *Nature* 486, 549–553.
- Cipolletta, D., Cohen, P., Spiegelman, B.M., Benoist, C., and Mathis, D. (2015). Appearance and disappearance of the mRNA signature characteristic of Treg cells in visceral adipose tissue: age, diet, and PPAR γ effects. *Proc. Natl. Acad. Sci. USA* 112, 482–487.
- Daluiski, A., Engstrand, T., Bahamonde, M.E., Gamer, L.W., Agius, E., Stevenson, S.L., Cox, K., Rosen, V., and Lyons, K.M. (2001). Bone morphogenetic protein-3 is a negative regulator of bone density. *Nat. Genet.* 27, 84–88.
- DeFronzo, R.A., Tripathy, D., Schwenke, D.C., Banerji, M., Bray, G.A., Buchanan, T.A., Clement, S.C., Henry, R.R., Hodis, H.N., Kitabchi, A.E., et al.; ACT NOW Study (2011). Pioglitazone for diabetes prevention in impaired glucose tolerance. *N. Engl. J. Med.* 364, 1104–1115.
- Fonseca, V. (2003). Effect of thiazolidinediones on body weight in patients with diabetes mellitus. *Am. J. Med.* 115 (Suppl 8A), 42S–48S.
- Fontaine, D.A., and Davis, D.B. (2016). Attention to background strain is essential for metabolic research: C57BL/6 and the international knockout mouse consortium. *Diabetes* 65, 25–33.
- Gouda, H.N., Sagoo, G.S., Harding, A.-H., Yates, J., Sandhu, M.S., and Higgins, J.P. (2010). The association between the peroxisome proliferator-activated receptor- γ 2 (PPARG2) Pro12Ala gene variant and type 2 diabetes mellitus: a huge review and meta-analysis. *Am. J. Epidemiol.* 171, 645–655.
- Hafemeister, C., and Satija, R. (2019). Normalization and variance stabilization of single-cell RNA-seq data using regularized negative binomial regression. *Genome Biol* 20, 296.
- Hevener, A.L., Olefsky, J.M., Reichart, D., Nguyen, M.T., Bandyopadhyay, G., Leung, H.Y., Watt, M.J., Benner, C., Febbraio, M.A., Nguyen, A.K., et al. (2007). Macrophage PPAR gamma is required for normal skeletal muscle and hepatic insulin sensitivity and full antidiabetic effects of thiazolidinediones. *J. Clin. Invest.* 117, 1658–1669.
- Hoffmann, J.M., Grünberg, J.R., Church, C., Elias, I., Palsdottir, V., Jansson, J.O., Bosch, F., Hammarstedt, A., Hedjazifar, S., and Smith, U. (2017). BMP4 gene therapy in mature mice reduces BAT activation but protects from obesity by browning subcutaneous adipose tissue. *Cell Rep.* 20, 1038–1049.
- Hsu, D.R., Economides, A.N., Wang, X., Eimon, P.M., and Harland, R.M. (1998). The *Xenopus* dorsalizing factor Gremlin identifies a novel family of secreted proteins that antagonize BMP activities. *Mol. Cell* 1, 673–683.
- Izumi, N., Mizuguchi, S., Inagaki, Y., Saika, S., Kawada, N., Nakajima, Y., Inoue, K., Suehiro, S., Friedman, S.L., and Ikeda, K. (2006). BMP-7 opposes TGF- β 1-mediated collagen induction in mouse pulmonary myofibroblasts through Id2. *Am. J. Physiol. Lung Cell. Mol. Physiol.* 290, L120–L126.
- Jaitin, D.A., Adlung, L., Thaiss, C.A., Weiner, A., Li, B., Descamps, H., Lundgren, P., Blierot, C., Liu, Z., Deczkowska, A., et al. (2019). Lipid-associated macrophages control metabolic homeostasis in a Trem2-dependent manner. *Cell* 178, 686–698.e14.
- Jurczak, M.J., Lee, A.-H., Jornayvaz, F.R., Lee, H.-Y., Birkenfeld, A.L., Guigni, B.A., Kahn, M., Samuel, V.T., Glimcher, L.H., and Shulman, G.I. (2012). Dissociation of inositol-requiring enzyme (IRE1 α)-mediated c-Jun N-terminal

- kinase activation from hepatic insulin resistance in conditional X-box-binding protein-1 (XBP1) knock-out mice. *J. Biol. Chem.* **287**, 2558–2567.
- Kim, D., Langmead, B., and Salzberg, S.L. (2015). HISAT: a fast spliced aligner with low memory requirements. *Nat. Methods* **12**, 357–360.
- Korchynski, O., and ten Dijke, P. (2002). Identification and functional characterization of distinct critically important bone morphogenetic protein-specific response elements in the *Id1* promoter. *J. Biol. Chem.* **277**, 4883–4891.
- Lehmann, J.M., Moore, L.B., Smith-Oliver, T.A., Wilkison, W.O., Willson, T.M., and Kliewer, S.A. (1995). An antidiabetic thiazolidinedione is a high affinity ligand for peroxisome proliferator-activated receptor gamma (PPAR gamma). *J. Biol. Chem.* **270**, 12953–12956.
- Levine, A.J., and Brivanlou, A.H. (2006). GDF3, a BMP inhibitor, regulates cell fate in stem cells and early embryos. *Development* **133**, 209–216.
- Levine, A.J., Levine, Z.J., and Brivanlou, A.H. (2009). GDF3 is a BMP inhibitor that can activate Nodal signaling only at very high doses. *Dev. Biol.* **325**, 43–48.
- Liao, Y., Smyth, G.K., and Shi, W. (2014). featureCounts: an efficient general purpose program for assigning sequence reads to genomic features. *Bioinformatics* **30**, 923–930.
- Lim, D.A., Tramontin, A.D., Trejevo, J.M., Herrera, D.G., García-Verdugo, J.M., and Alvarez-Buylla, A. (2000). Noggin antagonizes BMP signaling to create a niche for adult neurogenesis. *Neuron* **28**, 713–726.
- Lu, M., Sarruf, D.A., Talukdar, S., Sharma, S., Li, P., Bandyopadhyay, G., Nalbandian, S., Fan, W., Gayen, J.R., Mahata, S.K., et al. (2011). Brain PPAR- γ promotes obesity and is required for the insulin-sensitizing effect of thiazolidinediones. *Nat. Med.* **17**, 618–622.
- Majithia, A.R., Flannick, J., Shahinian, P., Guo, M., Bray, M.A., Fontanillas, P., Gabriel, S.B., Rosen, E.D., Altshuler, D., et al.; GoT2D Consortium; NHGRI JHS/FHS Allelic Spectrum Project; SIGMA T2D Consortium; T2D-GENES Consortium (2014). Rare variants in *PPARG* with decreased activity in adipocyte differentiation are associated with increased risk of type 2 diabetes. *Proc. Natl. Acad. Sci. USA* **111**, 13127–13132.
- Mao, T., Kusefoglou, D., Hooks, B.M., Huber, D., Petreanu, L., and Svoboda, K. (2011). Long-range neuronal circuits underlying the interaction between sensory and motor cortex. *Neuron* **72**, 111–123.
- Mayoral, R., Osborn, O., McNelis, J., Johnson, A.M., Oh, D.Y., Izquierdo, C.L., Chung, H., Li, P., Traves, P.G., Bandyopadhyay, G., et al. (2015). Adipocyte SIRT1 knockout promotes PPAR γ activity, adipogenesis and insulin sensitivity in chronic-HFD and obesity. *Mol. Metab.* **4**, 378–391.
- Mina, A.I., LeClair, R.A., LeClair, K.B., Cohen, D.E., Lantier, L., and Banks, A.S. (2018). CalR: a web-based analysis tool for indirect calorimetry experiments. *Cell Metab.* **28**, 656–666.e1.
- Morán-Salvador, E., López-Parra, M., García-Alonso, V., Titos, E., Martínez-Clemente, M., González-Pérez, A., López-Vicario, C., Barak, Y., Arroyo, V., and Clària, J. (2011). Role for PPAR γ in obesity-induced hepatic steatosis as determined by hepatocyte- and macrophage-specific conditional knockouts. *FASEB J.* **25**, 2538–2550.
- Nicholson, A., Reifsnyder, P.C., Malcolm, R.D., Lucas, C.A., MacGregor, G.R., Zhang, W., and Leiter, E.H. (2010). Diet-induced obesity in two C57BL/6 substrains with intact or mutant nicotinamide nucleotide transhydrogenase (*Nnt*) gene. *Obesity (Silver Spring)* **18**, 1902–1905.
- Odegaard, J.I., Ricardo-Gonzalez, R.R., Goforth, M.H., Morel, C.R., Subramanian, V., Mukundan, L., Red Eagle, A., Vats, D., Brombacher, F., Ferrante, A.W., and Chawla, A. (2007). Macrophage-specific PPAR γ controls alternative activation and improves insulin resistance. *Nature* **447**, 1116–1120.
- Parlee, S.D., Lentz, S.I., Mori, H., and MacDougald, O.A. (2014). Quantifying size and number of adipocytes in adipose tissue. *Methods Enzymol.* **537**, 93–122.
- Pauk, M., Bordukalo-Niksic, T., Brkljacic, J., Paralkar, V.M., Brault, A.L., Dumic-Cule, I., Borovecki, F., Grgurevic, L., and Vukicevic, S. (2019). A novel role of bone morphogenetic protein 6 (BMP6) in glucose homeostasis. *Acta Diabetol.* **56**, 365–371.
- Qian, S.W., Tang, Y., Li, X., Liu, Y., Zhang, Y.Y., Huang, H.Y., Xue, R.D., Yu, H.Y., Guo, L., Gao, H.D., et al. (2013). BMP4-mediated brown fat-like changes in white adipose tissue alter glucose and energy homeostasis. *Proc. Natl. Acad. Sci. USA* **110**, E798–E807.
- Ramírez-Zacarias, J.L., Castro-Muñozledo, F., and Kuri-Harcuch, W. (1992). Quantitation of adipose conversion and triglycerides by staining intracytoplasmic lipids with Oil red O. *Histochemistry* **97**, 493–497.
- Ray, A., and Dittel, B.N. (2010). Isolation of mouse peritoneal cavity cells. *J. Vis. Exp.* e1488.
- Robinson, M.D., McCarthy, D.J., and Smyth, G.K. (2010). edgeR: a Bioconductor package for differential expression analysis of digital gene expression data. *Bioinformatics* **26**, 139–140.
- Schneider, C.A., Rasband, W.S., and Eliceiri, K.W. (2012). NIH Image to ImageJ: 25 years of image analysis. *Nat. Methods* **9**, 671–675.
- Schreiber, I., Dörpholz, G., Ott, C.-E., Kragesteen, B., Schanze, N., Lee, C.T., Köhrlie, J., Mundlos, S., Ruschke, K., and Knaus, P. (2017). BMPs as new insulin sensitizers: enhanced glucose uptake in mature 3T3-L1 adipocytes via PPAR γ and GLUT4 upregulation. *Sci. Rep.* **7**, 17192.
- Schulz, T.J., Huang, P., Huang, T.L., Xue, R., McDougall, L.E., Townsend, K.L., Cypess, A.M., Mishina, Y., Gussoni, E., and Tseng, Y.-H. (2013). Brown-fat paucity due to impaired BMP signalling induces compensatory browning of white fat. *Nature* **495**, 379–383.
- Schulz, T.J., Graja, A., Huang, T.L., Xue, R., An, D., Poehle-Kronawitter, S., Lynes, M.D., Tolkachov, A., O’Sullivan, L.E., Hirshman, M.F., et al. (2016). Loss of BMP receptor type 1A in murine adipose tissue attenuates age-related onset of insulin resistance. *Diabetologia* **59**, 1769–1777.
- Scott, G.J., Ray, M.K., Ward, T., McCann, K., Peddada, S., Jiang, F.X., and Mishina, Y. (2009). Abnormal glucose metabolism in heterozygous mutant mice for a type I receptor required for BMP signaling. *Genesis* **47**, 385–391.
- Shen, J.J., Huang, L., Li, L., Jorgez, C., Matzuk, M.M., and Brown, C.W. (2009). Deficiency of growth differentiation factor 3 protects against diet-induced obesity by selectively acting on white adipose. *Mol. Endocrinol.* **23**, 113–123.
- Soccio, R.E., Chen, E.R., and Lazar, M.A. (2014). Thiazolidinediones and the promise of insulin sensitization in type 2 diabetes. *Cell Metab.* **20**, 573–591.
- Stechschulte, L.A., Czernik, P.J., Rotter, Z.C., Tausif, F.N., Corzo, C.A., Marciano, D.P., Asteian, A., Zheng, J., Bruning, J.B., Kamenecka, T.M., et al. (2016). *PPARG* post-translational modifications regulate bone formation and bone resorption. *EBioMedicine* **10**, 174–184.
- Stratton, I.M., Adler, A.I., Neil, H.A.W., Matthews, D.R., Manley, S.E., Cull, C.A., Hadden, D., Turner, R.C., and Holman, R.R. (2000). Association of glycaemia with macrovascular and microvascular complications of type 2 diabetes (UKPDS 35): prospective observational study. *BMJ* **321**, 405–412.
- Stuart, T., Butler, A., Hoffman, P., Hafemeister, C., Papalexi, E., Mauck, W.M.HaoY., 3rd, Stoekius, M., Smibert, P., and Satija, R. (2019). Comprehensive integration of single-cell data. *Cell* **177**, 1888–1902.e21.
- Tontonoz, P., and Spiegelman, B.M. (2008). Fat and beyond: the diverse biology of PPAR γ . *Annu. Rev. Biochem.* **77**, 289–312.
- Varga, T., Mounier, R., Patsalos, A., Gogolák, P., Peloquin, M., Horvath, A., Pap, A., Daniel, B., Nagy, G., Pintye, E., et al. (2016). Macrophage PPAR γ , a lipid activated transcription factor controls the growth factor GDF3 and skeletal muscle regeneration. *Immunity* **45**, 1038–1051.
- Wang, W., Yang, Y., Meng, Y., and Shi, Y. (2004). GDF-3 is an adipogenic cytokine under high fat dietary condition. *Biochem. Biophys. Res. Commun.* **321**, 1024–1031.
- Weir, J.B. (1949). New methods for calculating metabolic rate with special reference to protein metabolism. *J. Physiol.* **109**, 1–9.
- Yore, M.M., Syed, I., Moraes-Vieira, P.M., Zhang, T., Herman, M.A., Homan, E.A., Patel, R.T., Lee, J., Chen, S., Peroni, O.D., et al. (2014). Discovery of a class of endogenous mammalian lipids with anti-diabetic and anti-inflammatory effects. *Cell* **159**, 318–332.

STAR★METHODS

KEY RESOURCES TABLE

REAGENT or RESOURCE	SOURCE	IDENTIFIER
Antibodies		
rabbit anti-phospho-Akt Ser473	Cell Signaling Technology	4060S
rabbit anti-Akt	Cell Signaling Technology	9272S
rabbit anti- β -Tubulin	Cell Signaling Technology	2146
rat anti-Gdf3	R&D Systems	MAB953
mouse anti- β -Actin	Sigma Aldrich	A1978
rabbit anti-phospho-Smad2 Ser465/467/ Smad3 Ser423/425	Cell Signaling Technology	8828S
rabbit anti-Smad2	Cell Signaling Technology	5339S
rabbit anti-phospho-Smad1 Ser463/465/ Smad5 Ser463/465/ Smad9 Ser465/467	Cell Signaling Technology	13820S
rabbit anti-Smad1	Cell Signaling Technology	6944S
rabbit anti-Myc-Tag	Cell Signaling Technology	2278S
rabbit anti-phospho-PPAR γ Ser273	previously described (Choi et al., 2010)	N/A
mouse anti-PPAR γ	Santa Cruz	sc-7273
anti-rabbit IgG, Horseradish peroxidase- conjugated	Cell Signaling Technology	7074S
anti-mouse IgG, Horseradish peroxidase- conjugated	Cell Signaling Technology	7076S
anti-rat IgG, Horseradish peroxidase- conjugated	Cell Signaling Technology	7077S
anti-CD45.2 (clone 104)	BioLegend	109820
anti-CD45.1 (A20)	BioLegend	110706
anti-CD11b (M1/70)	BioLegend	141704
anti-F4/80 (BM8)	BioLegend	123114
anti-CD301 (LOM-14)	BioLegend	145709
anti-CD11c (N418)	eBioscience	61-0114-82
anti-SiglecF (E50-2440)	BD Biosciences	552126
anti-CD19 (6D5)	BioLegend	115508
anti-TCR- β (H57-597)	BioLegend	109222
anti-CD8 (53-6.7)	BioLegend	100730
anti-CD4 (RM4-5)	eBioscience	61-0042-82
anti-KLRG1 (2F1)	eBioscience	11-5893-82
anti-IL33R/ST2 (RMST2-2)	eBioscience	46-9335-82
Bacterial and Virus Strains		
AAV2/DJ-CAG-H2BGFP	Boston Children's Hospital viral core	N/A
AAV2/DJ-CAG-Gdf3	This manuscript	N/A
Chemicals, Peptides, and Recombinant Proteins		
Rosiglitazone, Cayman Chemical	Fisher Scientific	NC9560589
PD0325901	Selleckchem	S1036
Trametinib (GSK1120212)	Selleckchem	S2673
Recombinant mouse BMP4	R&D Systems	5020-BP-010
Critical Commercial Assays		
Ultra-Sensitive Mouse Insulin ELISA Kit	Crystal Chem	90080
NEBNext rRNA Depletion Kit	New England Biolabs	E6310X
NEBNext Ultra II Non-Directional RNA Second Strand Synthesis Module	New England Biolabs	E6111L

(Continued on next page)

Continued		
REAGENT or RESOURCE	SOURCE	IDENTIFIER
Nextera XT DNA Library Preparation Kit	Illumina	FC-131
Dual-Luciferase Reporter Assay System	Promega	E1960
High Capacity cDNA Reverse Transcription Kit, Applied Biosystems	Thermo Fisher Scientific	4368813
Foxp3 / Transcription Factor Staining Buffer Set, eBioscience	Thermo Fisher Scientific	00-5523-00
Deposited Data		
RNA-seq data	GEO repository	GEO: GSE151030
Experimental Models: Cell Lines		
Human: HEK293T	Spiegelman lab, Dana Farber Cancer Institute	N/A
Mouse: C2C12 C3H muscle myoblast	Sigma Aldrich	91031101
Experimental Models: Organisms/Strains		
Mouse: C57/Bl6J	The Jackson Laboratory	000664
Mouse: Bl6J PPAR $\gamma^{S273A/+}$	This manuscript	N/A
Mouse: B6.SJL-Ptprc ^a Pepc ^b /BoyJ	The Jackson Laboratory	002014
Oligonucleotides		
Primers for RT-qPCR analysis, see Table S1	This manuscript	N/A
Recombinant DNA		
pCMV6-Gdf3	This manuscript	N/A
pCMV6-Gdf3-Myc-Flag	OriGene Technologies	MR222967
pCMV6-Activin(Inhbb)-Myc-DDK	OriGene Technologies	MR225191
pAAV-CAG-GFP	Addgene	28014
Software and Algorithms		
CalR	Mina et al., 2018	https://calrapp.org/ ; RRID: SCR_015849
ImageJ	Schneider et al., 2012	https://imagej.nih.gov/ij/
Prism 8	GraphPad Software	https://www.graphpad.com/scientific-software/prism/
FlowJo	FlowJo, LLC	https://www.flowjo.com/
Other		
CLAMS indirect calorimeter	Columbus Instruments	http://www.colinst.com/

RESOURCE AVAILABILITY

Lead Contact

Further information and requests for resources and reagents should be directed to and will be fulfilled by the Lead Contact, Alexander S Banks (asbanks@bidmc.harvard.edu).

Materials Availability

All unique/stable reagents generated in this study are available from the Lead Contact with a completed Materials Transfer Agreement.

Data and Code Availability

RNA-seq data from eWAT of WT and A/A mice have been deposited in the Gene Expression Omnibus (GEO) repository under the accession number GEO: GSE151030.

EXPERIMENTAL MODEL AND SUBJECT DETAILS

Mouse Model

Generation of PPAR γ^{S273A} Mice

We obtained a C57BL/6 bacterial artificial chromosome (BAC) containing the *Ppar* locus (Invitrogen/RPCI). An 8.9 kb fragment preceding and including exon 5 was amplified by PCR (Phusion DNA Polymerase, NEB) and cloned into a plasmid encoding both a floxed

neomycin resistance cassette and a diphtheria toxin negative selection marker. Site-directed mutagenesis was used to alter the codon for serine 273 to alanine (TCA to GCA). Lastly, a 1.6 kb 3' homology arm was similarly amplified and cloned into the plasmid. C57BL/6 ES cells were electroporated with the linearized targeting construct. Using positive and negative selection, 8 ES cell clones were isolated and two were injected into BALB/c blastocysts. The resulting progeny gave rise to highly chimeric offspring. These chimeras were mated to C57BL/6J mice to obtain germline transmission of the mutant allele. To remove the floxed neomycin cassette, these germline offspring were crossed to mice expressing Cre in the female germline (Zp3-Cre). The progeny from these crosses were found to have deleted the neomycin cassette successfully. These heterozygous mice (PPAR γ ^{S273A/+}) were mated to generate homozygous knock-in mice PPAR γ ^{S273A/S273A} or PPAR γ ^{AVA}. Mice were backcrossed onto C57BL/6J for 6 generations, after which mice heterozygous for the PPAR γ ^{S273A} allele (PPAR γ ^{S273A/+}) were bred to generate experimental cohorts. The PPAR γ ^{S273A} allele was detected by PCR genotyping with primers 5'-CAGGAGGCTGAGCAGGTGTGTT-3', 5'-TCCAGACTGCCTTGGGAAAA-3', and 5'-AGCACACATGTACCCAACAT-3' (34 cycles, 96°C, 30 s; 65°C, 45 s; 72°C, 45 s), where the WT and knock-in alleles produced PCR products of 319 bp and 217 bp, respectively. To minimize phenotypic variability from a mixed 6J/6N background, PPAR γ ^{S273A/+} mice were genotyped for single nucleotide polymorphisms (SNPs) that distinguish between C57BL6/J and C57BL6/N alleles (Fontaine and Davis, 2016); mice homozygous for at least 9 SNPs specific to the C57BL/6J substrain on distinct chromosomes, including the 6/J null allele encoding nicotinamide nucleotide transhydrogenase (*Nnt*) (Nicholson et al., 2010), were used to establish cohorts for subsequent experiments.

Cell Lines

HEK293T cells (human female in origin) were cultured every 3 to 4 days using 0.05% Trypsin EDTA and maintained in DMEM (GIBCO, 11965118) supplemented with 10% heat inactivated FBS (FBS) and 1% Penicillin/Streptomycin. C2C12 myoblasts (ECACC, 91031101, C3H female mouse in origin) were cultured every 3 days using 0.25% Trypsin-EDTA and maintained in DMEM (GIBCO, 11965118) supplemented with 20% FBS and 1% Penicillin/Streptomycin. All cell lines were maintained at 37°C at 5% CO₂. Confluent C2C12 myoblast cells were induced to differentiate with serum withdrawal to 2% horse serum in collagen coated 6 well plates for 5 days. Differentiated C2C12 myotubes were returned to complete medium with 20% FBS for two days prior to subsequent experiments. These cell lines were not authenticated.

Primary Cell Culture

The stromal vascular fraction (SVF) containing preadipocytes and mononuclear cells were extracted from adipose tissue of WT or A/A mice (male) and cultured at 37°C with 5% CO₂. Cells were maintained in DMEM (GIBCO, 11965118) with 10% FBS and 1% Penicillin/Streptomycin until confluency. Two days post confluency, adipocyte differentiation was induced by treating cells (adipose tissue SVF) with 5 μ M dexamethasone, 250 μ M isobutylmethylxanthine, 1 μ M rosiglitazone, and 900 nM insulin in DMEM with 10% FBS and 1% Penicillin/Streptomycin for 48 h. Cells were maintained in culture medium containing FBS, Penicillin/Streptomycin, insulin, and rosiglitazone for another 2 days. Thereafter, cells were cultured in medium containing FBS and Penicillin/Streptomycin only.

METHOD DETAILS

Animal Experiments

All animal experiments were performed with approval from the Institutional Animal Care and Use Committees of The Harvard Center for Comparative Medicine, Brigham and Women's Hospital, and Beth Israel Deaconess Medical Center. Mice were maintained at 12 h/ 12 h light/ dark cycles, 22 \pm 2°C room temperature and 30%–70% humidity with *ad libitum* access to food and water, in individually ventilated cages. Cages and bedding were changed once every two weeks and mice were monitored regularly for their health status by animal technicians with the support of veterinary care and remained free of any adventitious infections for the entire duration of this study. Mice were fed a standard chow diet (13% kcal fat, LabDiet, no. 5053) or a HFD (60% kcal fat, Research Diets, no. D12492i) for the indicated durations. All experiments were performed in adult male mice (8 to 43 weeks of age). For HFD experiments, WT and AA mice were put on HFD at 6 weeks of age. Body composition of conscious mice were assessed with an EchoMRI 3-in-1 (Echo Medical Systems). At the end of experiments, mice were euthanized using CO₂, blood samples were collected via cardiac puncture in EDTA treated tubes on ice unless otherwise specified, and tissues were harvested and snap-frozen in liquid nitrogen and stored at –80°C until processing. Alternatively, samples of adipose tissue were fixed in formaldehyde, embedded in paraffin, sectioned and stained with H&E for determination of adipocyte area. Briefly, H&E stained slides were visualized and non-overlapping fields were captured for each sample using a Zeiss optical microscope and the AxioCam camera. Adipocyte area were calculated using ImageJ software (Schneider et al., 2012) using freely available macros described in Parlee et al. (2014). Adipocytes touching the edge of each image were excluded as well as cells < 350 μ m² as these cells may be a mixture of adipocytes and stromal vascular cells. For plasma collection, the blood samples in EDTA treated tubes were centrifuged at 2000 g at 4°C for 15 min, and the resulting supernatant was collected as plasma and stored at –80°C until processing. For measures of hematocrit, a small volume of whole blood was centrifuged in a microhematocrit capillary tube, and the height of the column of packed cells was expressed as a percentage of the height of the total blood column samples with visible hemolysis were excluded).

In Vivo AAV Experiments

12 week old male chow fed C57BL6/J mice were purchased from Jackson Labs and allowed to acclimate to our animal facility for 1 week. Each AAV was injected bilaterally into the quadriceps and gastrocnemius muscles at a dose of 1.5 \times 10⁸ vg in 30 μ L of PBS

per injection and into the epididymal fat depots at 2.5×10^8 vg in 50 μ L of PBS per injection. These viral injections were performed under isoflurane anesthesia and mice were given Buprenorphine SR Lab as the perioperative and postoperative analgesic prior to surgery at a dose of 0.5 mg/kg. These mice were maintained on chow and euthanized 9 weeks post injections.

Glucose and Insulin Tolerance Tests

Tests were performed on mice fasted for 16 and 4 h, respectively with *ad libitum* access to water. Following an initial blood glucose measurement post-fast, tolerance to an intraperitoneal (IP) injection of glucose (1–3 g/kg) or insulin (0.75–2 U/kg) was assessed by change in blood glucose over a period of 120 min. Glycemia was measured by tail vein bleeds at the indicated times using a Contour Next EZ glucometer (Bayer). Plasma insulin levels were measured using the Ultra-Sensitive Mouse Insulin ELISA Kit (Crystal Chem).

For PPAR γ ligand treatment prior to ITT, diet-induced obese mice were IP injected daily for 10 days with rosiglitazone (Cayman Chemical; 8 mg/kg) before insulin tolerance testing. Rosiglitazone was dissolved in dimethylsulfoxide (DMSO) and diluted into saline with 2% Tween-80 for injection. Administration of MEK inhibitors Trametinib and PD0325901 (Selleckchem) were as previously described (Banks et al., 2015). Mainly, Trametinib (3 mg/kg) or PD0325901 (10 mg/kg) were administered by daily oral gavage for 5 days. Compounds were dissolved in DMSO and diluted into an aqueous 250 μ L dose containing 0.5% hypromellose and 2% Tween-80.

Hyperinsulinemic-Euglycemic Clamp

WT and A/A mice fed HFD for 16 weeks were subjected to a hyperinsulinemic-euglycemic clamp study as previously described with minor modifications (Jurczak et al., 2012). Briefly, mice were allowed to recover for one week after an indwelling catheter was surgically implanted in the right jugular. Following an overnight fast of approximately 14 h mice were infused with a fixed amount of insulin [4 mU/(kg·min)] and a variable amount of 20% dextrose to maintain euglycemia (\sim 120 mg/dL). [3 - 3 H]glucose (PerkinElmer) was included in the infusate at a rate of 0.05 μ Ci/min for 2 h to allow for the calculation of whole-body rates of glucose metabolism. A 10- μ Ci bolus injection of 2-deoxy-D-[1- 14 C]glucose (10 μ Ci/mouse; PerkinElmer) was given at 90 min to determine tissue-specific glucose uptake. Blood was collected via tail massage for plasma glucose, insulin, and tracer levels at set time points during the 140-min infusion. For biochemical analysis of insulin signaling, obese mice of both genotypes were fasted for 4 h prior to IP injection of insulin (10 U/kg). Ten minutes after insulin injection, white adipose tissue, liver, and gastrocnemius were collected for subsequent protein analysis.

Indirect Calorimetry

For measurements of metabolic rate and food intake, we placed approximately 35 week old male mice fed HFD for 29 weeks within the CLAMS (Columbus Instruments) indirect calorimeter. Data from two independent cohorts was combined. One week prior to monitoring, mice were surgically implanted with wireless body temperature probes (Starr Scientific). Mice were acclimated for 13 h followed by 24 h measurement of VO_2 , VCO_2 , RER, locomotor and ambulatory activity, food intake at $23 \pm 0.1^\circ$ C while on HFD. Energy expenditure was calculated with the Weir equation (Weir, 1949). Calories consumed were calculated by multiplying hourly food intake by the 5.21 kcal/g caloric value of the 60% HFD. Energy balance was calculated by subtracting hourly food intake from hourly energy expenditure. Data from two separate experimental runs were combined. Results for locomotor activity ($n = 2$) and body temperature ($n = 3$) were removed due to equipment malfunction; other data from these animals were included. Analysis with ANOVA and ANCOVA were performed using CalR with the remove outliers feature activated (Mina et al., 2018).

Microquantitative Computed Tomography

For microCT analysis, a Scanco Medical μ CT 35 system with an isotropic voxel size of 7 μ m was used to image the femur. Scans were conducted in 70% ethanol using an X-ray tube potential of 55 kVp, an X-ray intensity of 0.145 mA and an integration time of 600 ms. Analysis was performed according to published guidelines (Bouxsein et al., 2010). From the scans of the femur, a region beginning 0.28 mm proximal to the growth plate and extending 1mm proximally was selected for trabecular bone analysis. A second region 0.6 mm in length and centered at the midpoint of the femur was used to calculate diaphyseal parameters. A semi-automated contouring approach was used to distinguish cortical and trabecular bone. The region of interest was thresholded using a global threshold that set the bone/marrow cut-off at 452.65 mg HA/cm 3 for trabecular bone and 579.86 mg HA/cm 3 for cortical bone. 3-D microstructural properties of bone, including TMD and bone volume fraction (BV/TV), were calculated using software supplied by the manufacturer.

RNA Isolation and Gene Expression Analysis by qPCR, RNA-seq, or Single Cell RNA-seq

RNA Isolation

For experiments utilizing RNA-seq or qPCR, total RNA was isolated from cells or tissues using TRIzol reagent (Thermo Fisher) followed by a Direct-zol RNA MiniPrep kit (Zymo Research) according to the manufacturer's instructions. The RNA was reverse-transcribed using Multiscribe Reverse Transcriptase and a high-capacity cDNA reverse transcription kit (Applied Biosystems).

Quantitative Real-Time PCR (qPCR)

Quantitative real-time PCR (qPCR) was performed using synthesized cDNA with SYBR Select Master Mix (Applied Biosystems) on a Light Cycler 480 II (Roche) or the QuantStudio 5 Real-Time PCR System (Applied Biosystems). Relative mRNA expression was determined by the $\Delta\Delta$ -C $_t$ method normalized to TATA-binding protein (TBP) levels. The list of primers used in this study is included in Table S1.

RNA-sequencing (RNA-seq)

400ng of total RNA was used as input for RNA-seq Library construction, which consisted of rRNA removal via the NEBNext rRNA depletion kit and conversion to cDNA using the NEBNext Ultra II Non-Directional RNA Second Strand Synthesis Module, both per manufacturer's instructions. cDNA was diluted 1:15 and subsequently tagmented and amplified for 12 cycles using the Nextera XT DNA Library Preparation Kit (Illumina). Individual libraries were QC'd by Qubit and Agilent Bioanalyzer, pooled, and sequenced at a final loading concentration of 1.8 pM on a NextSeq500 (36bp x 36bp paired-end reads). Sequencing reads were demultiplexed using bcl2fastq (v2.20.0) and aligned to the mm10 mouse genome by with HISAT2 (v. 2.0.5; Kim et al., 2015). PCR duplicates and low-quality reads were filtered by Picard (<https://broadinstitute.github.io/picard>). Filtered reads were assigned to the annotated transcriptome and quantified using featureCounts (Liao et al., 2014). Normalization and differential expression analysis were performed using EdgeR (v 2.9.2) (Robinson et al., 2010).

Single Cell RNA-seq

Identification of Gdf3-expressing cells in HFD-fed mice was performed using single cell RNA-sequencing from SVF fraction of eWAT of mice by Jaitin et al. (2019). These data were clustered *de novo* using the SCTransform seurat pipeline (Hafemeister and Satija, 2019; Stuart et al., 2019) using the following parameters: 2000 variable genes, 25 UMAP and SNN dimensions, and clustering resolution of 0.4. Excluded from analysis were a list of mitochondrial and ribosomal genes identified by Jaitin et al. (2019).

Preparation of Cell or Tissue Lysates and Immunoblotting

Whole-cell extracts were prepared in RIPA lysis buffer containing 50 mM Tris pH 7.5, 150 mM NaCl, 1% NP-40, 0.5% sodium deoxycholate, 0.1% SDS, and 1 × HALT protease and phosphatase inhibitor cocktail (Thermo Fisher). For tissue lysates, frozen tissue was pulverized in liquid nitrogen followed by homogenization in lysis buffer using stainless steel ball bearings and a TissueLyser (QIAGEN). Protein concentration was determined by Pierce BCA protein assay (Thermo Fisher) and lysates separated by SDS-PAGE with Mini-PROTEAN TGX gels (Bio-Rad), transferred to PVDF membranes using the Trans-Blot Turbo transfer system (Bio-Rad), and blotted according to manufacturer's recommendations for the indicated antibodies. Primary antibodies used in this study include: rabbit anti-phospho-Akt Ser473, rabbit anti-Akt, rabbit anti-β-Tubulin, rat anti-Gdf3, mouse anti-β-Actin, rabbit anti-phospho-Smad2 Ser465/467/ Smad3 Ser423/425, rabbit anti-Smad2, rabbit anti-phospho-Smad1 Ser463/465/ Smad5 Ser463/465/ Smad9 Ser465/467, rabbit anti-Smad1, rabbit anti-Myc-Tag, rabbit anti-phospho-PPAR γ Ser273, and mouse anti-PPAR γ . Horse-radish peroxidase-conjugated secondary antibodies were obtained from Cell Signaling Technologies. Chemiluminescence assays were performed using SuperSignal West Dura extended duration substrates (Thermo Fisher) and detected with a ChemiDoc XRS+ or ChemiDoc Touch Imaging System (Bio-Rad). Image analyses were performed using Image Lab software (Bio-Rad).

DNA Constructs and AAVs

A non-tagged construct of mouse Gdf3 was generated using the commercial vector pCMV6-Gdf3-Myc-Flag (OriGene Technologies, MR222967), containing a Myc-Flag-tagged Gdf3, and PCR-based mutagenesis to introduce a STOP codon upstream of the C-terminal Myc-Flag tag. The BMP responsive element luciferase reporter, derived from the ID1 luciferase reporter (Korchynskyi and ten Dijke, 2002) was provided by C. Brown. A Myc-Flag-tagged mouse Activin expression plasmid was purchased from Origene Technologies (MR225191). AAV Gdf3 was generated by subcloning non-tagged Gdf3 into the AAV2/1 vector backbone of AAV-CAG-GFP, a gift from Karel Svoboda via Addgene plasmid 28014 (Mao et al., 2011). Viral packaging into the AAV-DJ serotype and titer determination were performed by the Boston Children's Hospital Viral Core. Premade control AAV2/DJ-CAG-H2BGFP virus (AAV-GFP) was purchased from the same core facility.

Lipid Accumulation Assay

Lipid accumulation in adipocytes was detected by Oil Red O staining as described (Ramírez-Zacarias et al., 1992).

Glucose Uptake Assays

C2C12 myoblast cells were differentiated and transduced with either AAV-GFP or AAV-Gdf3 (1.2×10^{10} vg per well in a 48 well plate) and (1.2×10^{11} vg per well in 6 well plates). Approximately 36 h post transduction, the cells from the 6 well plates were incubated in serum-free DMEM for 3 h at 37°C, incubated with or without 200 nM insulin for 20 min washed twice in ice cold PBS and lysed with RIPA lysis buffer for western blot analysis as described above. The cells from the 48 well plate were used for glucose uptake assays using the protocol described in Yore et al. (2014) with minor modifications. Briefly, cells were washed twice with serum-free DMEM and incubated in serum-free DMEM for 3 h at 37°C. Cells were then washed 3 times with Krebs-Ringer-HEPES (KRH) buffer (50 mM HEPES pH 7.4, 137 mM NaCl, 1.25 mM CaCl₂, 4.7 mM KCl, 5.0 mM, 1.25 mM MgSO₄). Cells were incubated in KRH for 30 min then incubated in KRH with or without 200 nM insulin for 20 min before the addition of a deoxy-D-glucose, 2-[1,2-³H (N)]/2-deoxy-D-glucose solution, yielding final assay concentrations of 1 μ Ci of [³H] 2-deoxy-D-glucose and 100 μ M 2-deoxy-D-glucose per well. After 5 min the KRH buffer was removed immediately by aspiration. Cells were washed 3 times in ice-cold PBS to inhibit further glucose uptake and wash away unincorporated radiolabeled [³H] 2-deoxy-D-glucose. Cells were solubilized with 0.5% SDS. Half of the lysates from each well were used to assay [³H] disintegration levels by liquid scintillation counting and the other half was used for normalization to protein concentrations.

Luciferase Reporter Assays

C2C12 myoblasts were transfected without myogenic differentiation. HEK293T or C2C12 cells were transfected with a firefly luciferase reporter construct and a fixed amount of DNA, as normalized with empty vector plasmid using Lipofectamine 2000 and 3000 transfection reagents (Invitrogen), respectively, according to the manufacturer's recommendations. Luciferase activity was measured 24–48 h after transfection using the Dual-Luciferase Reporter Assay system (Promega), with quantification of luminescence on a FLUOstar OPTIMA plate reader (BMG Labtech). Co-transfection of CMV-driven *Renilla* luciferase vector was used to normalize for transfection efficiency. Where indicated, cells were rinsed with PBS and switched to DMEM lacking serum prior to luciferase measurement. As a positive control for BMP signaling, recombinant protein of mouse BMP4 (R&D Systems) was added to the medium 16 h before analysis.

Isolation of Macrophages

Peritoneal macrophages were harvested from chow fed, 15 to 20 week old mice as previously described (Ray and Dittel, 2010). Briefly, WT or A/A mice were given an IP injection of 3% thioglycolate solution (3 mL per mouse). 4 days post injection, mice were euthanized and their peritoneal cavity was carefully injected with 5 mL of ice cold PBS (with 3% FBS) using a 27G needle without puncturing any organs. The peritoneum was gently massaged to dislodge any attached cells into the PBS solution which was then aspirated using a 25G needle attached to a 5mL syringe. These peritoneal cells were collected into ice cold 50mL polypropylene tubes, erythrocytes were lysed using ACK lysis buffer (GIBCO), resuspended in ice cold PBS (with 3% FBS) and centrifuged for 8 min at 400 g at 4°C. The pelleted cells were resuspended in DMEM containing 10% FBS and allowed to adhere for 2 h in 10cm cell culture dishes in a 37°C incubator with 5% CO₂. Nonadherent cells were washed away with PBS, and adherent cells were scraped and used as peritoneal macrophages for further experiments.

Isolation of Cells from SVF

The stromal vascular fraction (SVF) containing preadipocytes and mononuclear cells was extracted from adipose tissue. For isolation of preadipocytes, inguinal adipose tissue was digested in a PBS buffer containing 10 mg/mL collagenase D (Roche), 2.4 U/mL dispase II, and 10 mM CaCl₂ for 45 min shaking at 37°C. Digestion was neutralized with culture medium consisting of DMEM/F12 supplemented with 10% FBS and penicillin/streptomycin. Cell suspensions were filtered through 100 μm and 40 μm cell strainers, and the SVF cells resuspended in growth medium for expansion. For isolation of mononuclear cells and subsequent immunophenotyping, epididymal and inguinal adipose tissues were digested for 20–30 min at 37°C with collagenase type II (Sigma). Cell suspensions were filtered through a sieve, and the SVF fraction was collected after red blood cell lysis (ACK Lysing Buffer, GIBCO) and filtration through a 40 μm cell strainer.

Immunophenotyping and Flow Cytometry

Adipose tissue SVF cells were resuspended in FACS buffer (phenol red-free DMEM supplemented with 10 mM HEPES and 2% FCS) and incubated for 30–45 min at 4°C with Fc block and the indicated fluorescence-labeled antibodies for surface molecule staining. For myeloid cell analysis, cells were stained with anti-CD45.2 (clone 104), -CD45.1 (A20), -CD11b (M1/70), -F4/80 (BM8), and -CD301 (LOM-14) antibodies from BioLegend; -CD11c (N418) antibody from eBioscience; and -SiglecF (E50-2440) antibody from BD Biosciences. For lymphoid cell analysis, cells were stained with anti-CD45.2, -CD45.1, -CD19 (6D5), -TCR-β (H57-597), and -CD8 (53-6.7) antibodies from BioLegend; -CD4 (RM4-5), -KLRG1 (2F1), and -IL33R/ST2 (RMST2-2) antibodies from eBioscience; and were fixed, permeabilized and intracellularly stained for Foxp3 (FJK-16 s) according to the manufacturer's instructions (eBioscience). Dead cells were excluded by staining with a fixable LIVE/DEAD dye (ThermoFisher). Cells were analyzed using an LSRII instrument (BD Bioscience) and FlowJo software.

Bone Marrow Transplantation

Bone marrow progenitor cells were isolated by flushing femurs and tibiae of 10 to 12 week old donor animals with PBS, and T cells depleted from BM by magnetic beads. Recipient mice between 8 to 12 weeks of age were irradiated with 1000 rads prior to reconstitution with 3–5 × 10⁶ donor cells by retro-orbital injection. Irradiated mice were kept in sterile cages with standard chow diet and antibiotic-treated water for 2 weeks. After 4 weeks recovery, mice were bled to monitor reconstitution and started on HFD treatment for an additional 20 weeks. To distinguish chimerism, transplantation studies made use of congenic C57BL/6 strains carrying functionally equivalent alleles of the pan leukocyte marker CD45. For studies with PPAR $\gamma^{+/+}$ recipient mice, mice harboring the CD45.1 allele were purchased from Jackson (B6.SJL-Ptprc^aPepp^b/BoyJ) and transplanted with bone marrow from PPAR $\gamma^{+/+}$ or PPAR $\gamma^{A/A}$ mice, which carry the WT allele for CD45 (CD45.2). For studies with PPAR $\gamma^{A/A}$ recipient mice, PPAR $\gamma^{A/A}$ mice were transplanted with bone marrow from PPAR $\gamma^{+/+}$ or PPAR $\gamma^{A/A}$ mice heterozygous for CD45.1.

QUANTIFICATION AND STATISTICAL ANALYSIS

Data were analyzed using Prism software (GraphPad Software) and are expressed as mean ± SEM. All data were assumed to have a normal distribution and two-tailed Student's t tests, one-way ANOVA with Newman-Keuls Multiple Comparison test, or two-way ANOVA were used to compare means between groups as indicated in the figure legends; p < 0.05 was considered significant.